Targeted Nanoparticle Drugs with Immunotherapy Against Bladder and Breast Cancer

By

SARA ABOU-ADAS
THESIS

Submitted in partial satisfaction of the requirements for the degree of

MASTER OF SCIENCE

in

Pharmacology and Toxicology

in the

OFFICE OF GRADUATE STUDIES

of the

UNIVERSITY OF CALIFORNIA

DAVIS

Approved:

_____
Kit S. Lam, Chair

_____
Yuanpei Li

_____
Jeremy Chien

Committee in Charge

2024

Table of Contents

Acknowledgements

The completion of this thesis owes its success to the generous support and assistance of numerous individuals, whom I would like to sincerely thank. My deepest gratitude goes to my esteemed Masters advisor and PI, Dr. Kit Lam, whose unwavering support and expert guidance over the past four years have been instrumental in my academic journey at UC Davis. Dr. Lam's encouragement, passion for research, and opportunities for collaboration and conference participation have broadened my perspective and sharpened my problem-solving skills. Beyond academia, his caring demeanor has provided invaluable support during challenging times. I am also grateful to my committee members, Dr. Yuanpei Li and Dr. Jeremy Chein, for their support, constructive feedback, and time dedicated to reviewing my thesis. Special thanks are extended to the faculty of the Department of Biochemistry and Molecular Medicine at UC Davis, particularly Dr. Ai-Hong Ma, Dr. Junwei Zhao, and Dr. Urvashi Bhardwaj, for their invaluable teachings and mentorship throughout my studies.

Lastly, my heartfelt appreciation goes to my family for their unwavering love, support, and guidance, which have been my compass in navigating life's journey.

Abstract of Thesis

Smart nanoparticles differ from conventional nanoparticles due to their capability of reacting or being directed to biological signals for precise targeted drug delivery to the tumor microenvironment[1] and therefore are emerging as a highly promising platform for precise cancer treatment. With the rapid progression of multi-drug resistance and metastasis, smart nanoparticles offer rapid advancements in different treatment modalities for oncology. An ideal smart nanoparticle should meet several basic criteria, such as stimulus responsive material or structure, stable nanometer size, adjustable surface charge, high encapsulation capacity, biocompatibility, degradability, and low toxicity, etc.[1] Equipped with tumor targeting ligand and stimulus responsive elements, these smart nanoparticles can preferentially accumulate in the tumor microenvironment and release the chemotherapeutic agents. Moreover, their capacity for co-delivering both therapeutics and diagnostic agents can significantly propel the advancement of personalized medicine.

This thesis focuses on two different platforms of smart nanoparticle therapy coupled with immunotherapy, illustrated by two different projects and each is explained in one chapter. Chapter 1 discusses a self-assembling micelle designed to deliver an immunomodulator and a photosensitizer, while being decorated with PLZ4, a bladder cancer- targeting ligand. This ligand selectively targets αvβ3 integrin over-expressed on surface of bladder cancer cell lines as well as all five primary bladder cancer cells sourced from human patients, exhibiting no affinity for normal urothelial cells. Chapter 2 explores a different drug-delivery platform that utilizes the endogenous protein, human albumin serum (HSA). This vehicle is site-specifically modified with two targeting

ligands: LBF127, which locates surface receptors present in triple-negative breast cancer cells, and LLP2A, which attaches to α4β1 integrin on activated NK cells and T-cells. This modification results in an amplified synergistic anti-tumor effect overall through the targeted delivery and accumulation of bortezomib, a potent proteosome inhibitor currently used in the clinic.

Chapter 1: Targeted Nanoparticle Drug with Immunotherapy and Phototherapy Against Bladder Cancer

1.1 Abstract

Our aim is to develop an effective bladder cancer-targeting nanoparticle capable of delivering the immunomodulator, imiquimod, and a photosensitizer, indocyanine green derivative (ICGD), specifically to bladder cancer sites for phototherapy (PT) and immunotherapy. This phototherapy will encompass both photodynamic effects and photothermal heat effect. Here, we report the development of a self-assembling micelle that is decorated with the targeting ligand, PLZ4. This micelle is designed to selectively target and attach to αvβ3 integrin, which is overexpressed in urothelial carcinoma cells, facilitating the delivery of imiquimod and ICGD to the tumor sites. Once the tumor cell internalizes the photosensitizer, phototherapy can be applied to induce the generation of reactive oxygen species (ROS), activating apoptotic pathways mechanistically. As a result, we anticipate observing a notable anti-tumor effect and prolonged survival in vivo.

1.2 Introduction

Bladder cancer is within the 10 most common types of cancer, ranking as the fourth most common cancer in men and the eleventh most common in women worldwide.[1,2] Urothelial cell carcinoma accounts for 90% of all bladder cancer cases, meanwhile squamous cell carcinoma only accounts for 5% of these cases.[1] There is a medical need to develop a treatment that can selectively target local and metastatic bladder cancer cells, while still maintaining healthy surrounding cells. While different

treatments exist for urothelial cell carcinoma, the challenge persists to overcome drug resistance to immunotherapy and chemotherapy.

Zhang et al. initially developed the bladder cancer-targeting peptide named PLZ4, a cyclic peptide (amino acid sequence: cQDGRMGFc) that selectively binds to αvβ3 integrin in bladder cancer cell lines and all the five primary bladder cancer cells from human patients, but not to normal urothelial cells, cell mixtures from normal bladder specimens, fibroblasts, and blood cells.[4] Subsequently, Zhu et al. engineered a porphyrin-based nanometer-scale micelles embellished with cancer-specific targeting PLZ4 on the surface.

Our micellar nanoparticle, referred to as a PLZ4-ICGD-Imiquimod (or PLZ4-ICGD-Imiq) is constructed from amphiphilic polymer building blocks called telodendrimers. These telodendrimers consist of a backbone of polyethylene glycol (PEG) linked to dendritic lysines, each possessing 8 terminal primary amines, to which cholic acid or indocyanine green derivative (ICGD) can be attached. On the terminal end of the PEG chain, a bladder cancer-specific ligand named PLZ4 is attached. To create PLZ4-ICGD-Imiq, imiquimod was dissolved in a 3:1 ratio of Dichloromethane/Methanol containing three distinct telodendrimers (PLZ4-PEG^{5k}-Lys_7-CA_8, MeO-PEG^{5k}-Lys_7-Cys_4-CA_8, and MeO-PEG^{5k}-Lys_7-$ICGD_4$-CA_4) (Figure 1). After rotoevaporation, a thin film is formed on the wall of the round-bottom flask, saline was added to generate micellar PLZ4-ICGD-Imiq, which can be used for combination phototherapy and immunotherapy, in addition to other therapeutic modalities.[5]

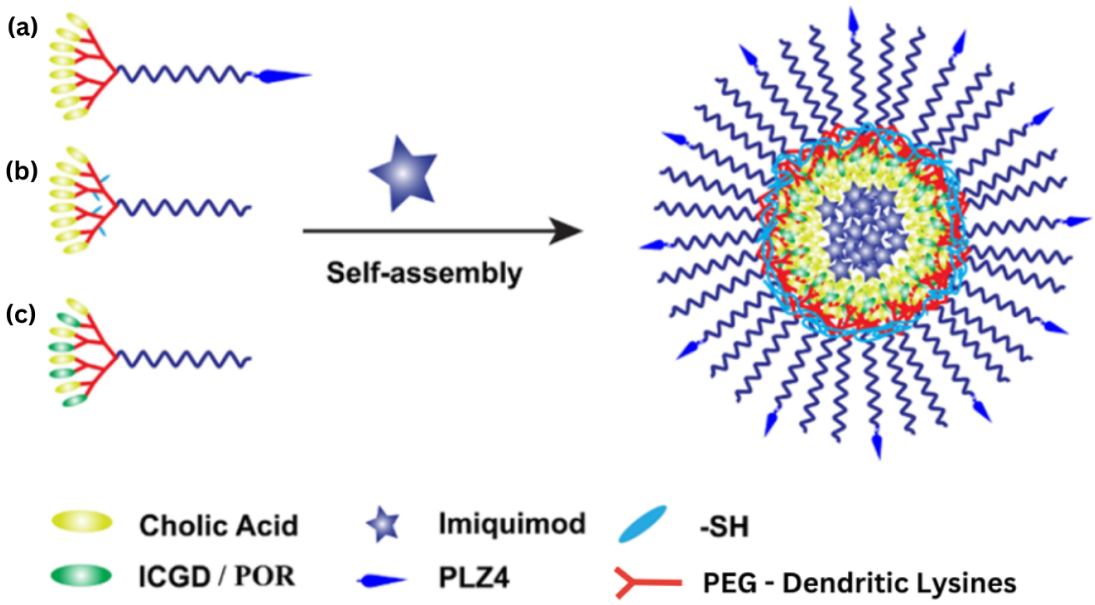

Figure 1: Cartoon schematic of proposed targeting nanoparticle (PLZ4-ICGD-Imiq) self-assembling into a micelle. PLZ4-conjugated telodendrimers: (a) (PLZ4-PEG^{5k}-Lys$_7$-CA$_8$), (b) cystine-containing telodendrimers (MeO-PEG^{5k}-Lys$_7$-Cys$_4$-CA$_8$, and (c) indocyanine green derivative-containing telodendrimers (MeO-PEG^{5k}-Lys$_7$-ICGD$_4$-CA$_4$).

Phototherapy encompasses both photodynamic effects, which generate reactive oxygen species, and photothermal heat. Photodynamic therapy (PDT) functions by utilizing a photosensitizer that accumulates within tumor cells, followed by exposure to light of a matching wavelength. This process generates reactive oxygen species, initiating apoptosis and effectively destroying cancer cells.[6] Photodynamic therapy is especially advantageous for treating bladder cancer due to its hollow organ structure accessible via the urethra, which allows for homogenous light delivery through diffusing fibers. In this project, indocyanine green derivative (ICGD) acts as a photosensitizer that can be activated by light at a wavelength of 808 nanometers. Figure 2, shows neoplastic cancerous growths in the bladder wall. Following intravenous administration, the described nanoparticle accumulates in the tumor masses within 24 hours. A laser probe is then guided through the urethra until it reaches the bladder cavity, enabling the

illumination of light. This procedure initiates the generation of reactive oxygen species (ROS), which in turn activate apoptotic pathways.[6]

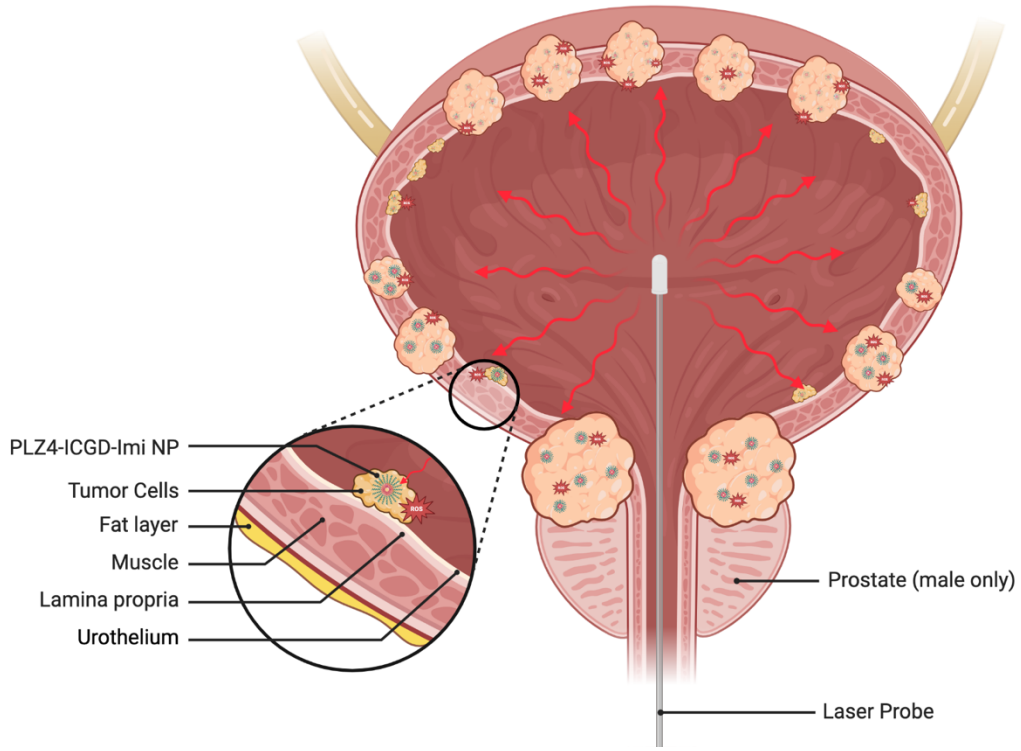

Figure 2: Targeted Bladder Cancer Nanoparticle Delivery with Phototherapy Activation. Cartoon schematic representing a bladder exhibiting neoplastic cancerous growths. After 24 hrs post i.v., the discussed nanoparticle accumulates in the tumor masses and a laser probe is navigated through the urethra until it reaches the hollow organ, where light can be shined. This process generates reactive oxygen species (ROS), which activate apoptotic pathways.

Immune response modifiers (IRMs) and immune checkpoint inhibitors (ICIs) are notable for their direct and indirect mechanism of actions on the innate and adaptive immune systems to further enhance the host's natural immune response against cancer cells.[7,8] Among these IRMs is imiquimod, which operates via dendritic cells expressing toll-like receptor 7 (TLR-7), to trigger an immune cell-mediated anti-tumor effect.[9] Following activation of nuclear factor-κB, which once released from its inhibitor, translocates to the nucleus, prompting the transcription of diverse cytokines and

chemokines.[9] Another component of our proposed treatment regimen entails utilizing an immune checkpoint inhibitor called anti PD-1. This medication works by disrupting the communication between programmed cell death protein 1 (PD-1) on T cells and its corresponding ligand PD-L1, which is often overexpressed by cancer cells. By preventing ligand binding to PD-1, this inhibition removes the regulatory constraints on the immune system, enabling T-cells to recognize cancer cells more effectively and vigorously in order to promote a durable anti-tumor immune response.[8] Hsu et al. investigated whether photoimmunotherapy could sensitize checkpoint inhibitor-resistant tumors to anti-PD-1 agents. They found that while anti-PD-1 monotherapy failed to inhibit tumor growth, photoimmunotherapy alone reduced growth and prolonged survival. Furthermore, the combination treatment significantly enhanced these effects, indicating potential sensitization of anti-PD-1 resistant tumors.[10] Therefore, our study incorporates anti-PD-1 as part of a triple combination therapy regimen alongside phototherapy and immune response modifiers.

1.3. MATERIALS AND METHODS

Biodistribution

UPII-SV40 T and UPII-Ras double-transgenic FVB mice carrying spontaneous bladder cancer were treated approximately 3-5 weeks post birth. PLZ4-ICGD-Imiquimod [based on the concentration of PCNP:Imiq/kg (75mg:1.875mg) was i.v. administered via tail vein to transgenic FVB mice carrying spontaneous bladder cancer. The biodistribution was evaluated by Spectral Lago X *in vivo* imaging system, and *ex vivo* imaging of the excised organs and tumor tissues. For *ex vivo* imaging, the UPII-SV40 T and UPII-Ras double-transgenic FVB mice were sacrificed at 6, 24, 48, 72, 96, and 120

hours (n = 3 for each time point). Tumors and organs were harvested for near infrared fluorescence imaging. The best signal-to-noise ratio was obtained using the excitation/emission wavelength pair of 810/850 nm, and thus, this setting was used for the imaging of both whole body and organs.

Hematologic Analysis

Healthy, non-tumor bearing, female mice, between 6-8 weeks of age, were chosen due to the constraints posed by the longer length of the male urethra during intravesical light treatment. Various concentration of PLZ4-ICGD-Imiquimod were used at the doses of PLZ4-ICGD:imiquimod/kg body weight (50mg:1.25mg/kg, 75mg:1.875mg/kg, 100mg:2.5mg/kg, 150mg:3.75mg/kg, 200mg:5mg/kg) and administered to the mice via tail vein injection. Twenty-four hours after nanoparticle dosing, mice were treated with intravesical phototherapy. The duration and dose of laser irradiation was 2 min at 0.2 Wcm^{-2} (808 nm). The mice from each group were sacrificed on day 3, day 10 and day 17 to test complete blood count (CBC) and complete metabolic count (CMP) parameters determined by Heska Hematology Analyzer. Upon animal anesthesia, blood was collected retro-orbitally and split between EDTA tubes and empty eppendorf tubes. Plasma of the blood samples were obtained by centrifuging at 12,000 min^{-1} for 10 min and the blood chemistry parameters were determined using Heska DRI-CHEM veterinary blood chemistry analyzer. Blood results were compared between normal FVB reference ranges from Jackson Labs[11], Taconic Biosciences[12], and Schneck et al.[13]. Animal body weights were recorded every other day during the course of observation.

Transgenic Breeding and Survival Study

Using tail snips, genotyping was conducted before day 21 by polymerase chain reaction (PCR) using the following primers:

RAS-F: TCCCACTCCGAGACAAAATC, RAS-R: ATTCGTCCACGAAGTGGTTC, SV40T-F: GGAAAGTCCTTGGGGTCTTC, SV40T-R: CACTTGTGTGGGTTGATTGC. Based on the genotyping results (Fig. 3), mice were identified to carry heterozygous UPII-Ras* (Ras with codon 61 mutation Q > L) and heterozygous UPII-SV40T transgenes were crossbred to generate double transgenic mice. Due to technical challenges associated with bladder insertion of an optical fiber in male mice for PDT, only female double transgenic mice were utilized and randomly assigned to the following 12 groups:

Treatment Groups *(PLZ4-ICGD = NP)*		
PBS (Control)	Anti-PD-1	Laser Only
NP-Imiq + Laser +anti PD-1	NP + Laser + anti PD-1	NP-Imiq + Anti PD-1
NP-Imiq + Laser	NP + Laser	NP + Anti PD-1
NP-Imiq	NP	Laser + Anti PD-1

The prepared nanoparticle was diluted by 2-fold using 2xPBS to make a working solution of polymer (10 mg) to imiquimod (0.25 mg) per mL in PBS. PLZ4-ICGD-Imiq or PLZ4-ICGD was administered intravenously on days 1, 8, and 15, followed by intravesical laser treatment 24 hours later. Prior to phototherapy, the outer skin was sanitized with alcohol wipes and the mice urethras were flushed with PBS using a dull tip catheter needle. The intravesical bladder phototherapy was administered using a glycerol lubricated 400 micron ball-tip optical fiber and 808 nm laser for 3 minutes, at

0.2 W/cm². Anti PD-1 treatment was administered on days 2, 9, and 16. Tumor progression was monitored using magnetic resonance imaging (MRI) on a weekly basis until mortality. Animal weights were monitored on a weekly basis until natural death or humane endpoints were reached.

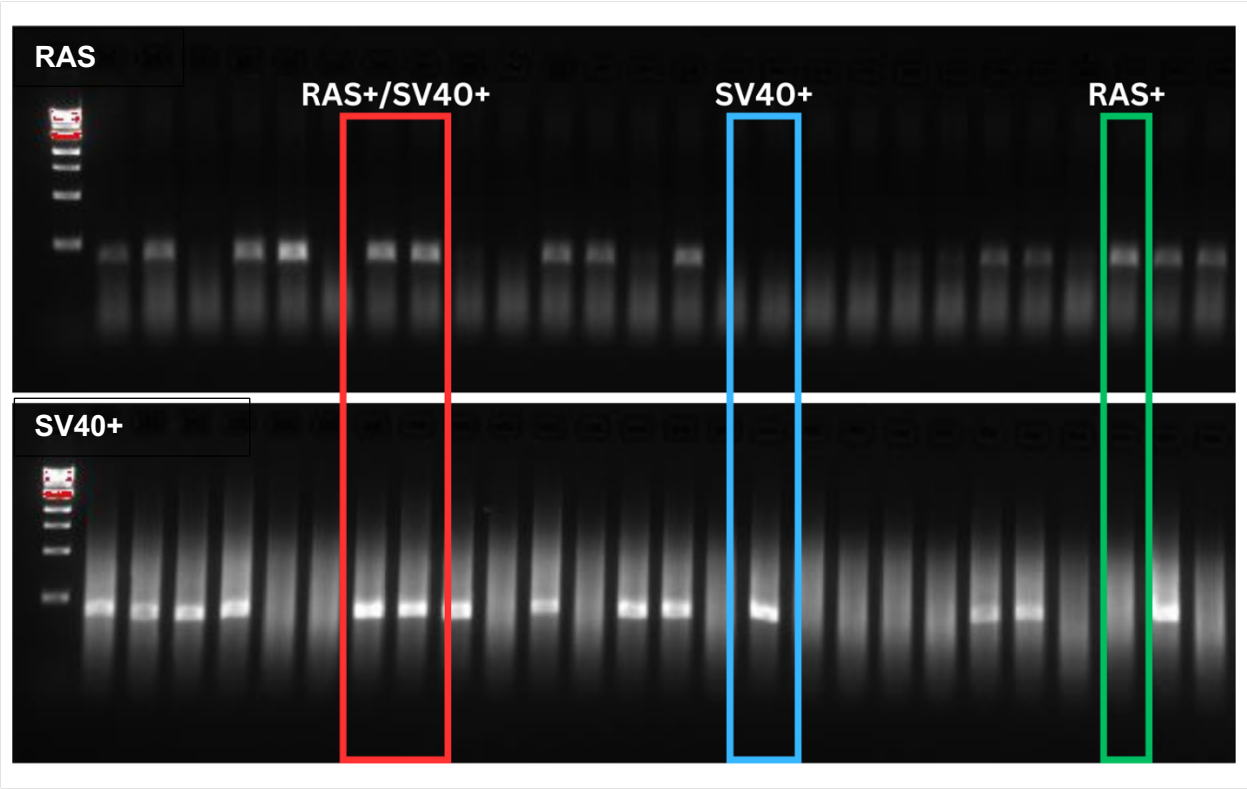

Figure 3: **Genotyping of transgenic mice. Tails were snapped and DNA was extracted for polymerase chain reaction (PCR) amplification of the RAS (top panel) and SV40+ (bottom panel) gene fragments. Red box outlines double positive transgenic mice.**

Anti-Tumor Efficacy Study in MB49 metastatic cancer mouse model

C57BL/6 mice (60 female and 60 male) were inoculated subcutaneously on both flanks with half a million MB49-GFP-Luc murine bladder cancer cells (day -6). Weekly treatment cycle involved IV drug on day 1, phototherapy on day 2, and anti-PD1 on day 3. A total of 2 treatment cycles were administered and tumor volumes were observed every 3-4 days (Fig. 4). Photothermal images were also documented to observe

localized temperature increase in thirty second increments for each phototherapy session.

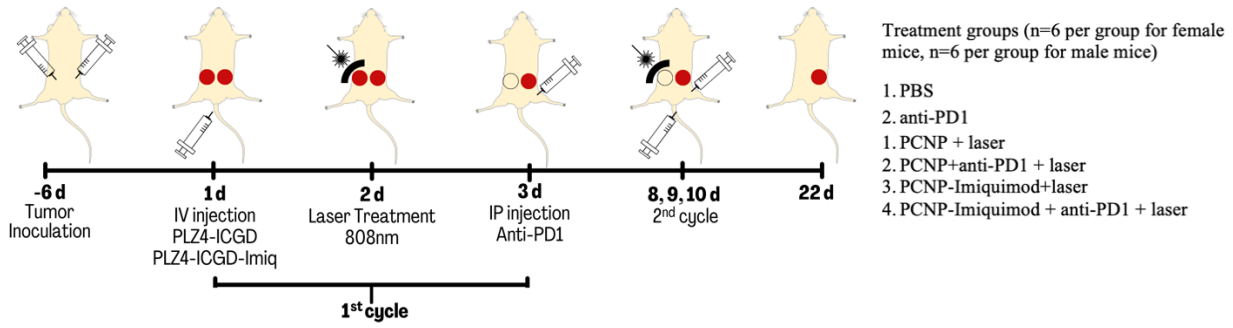

Figure 4. Schematic illustration of PLZ4-ICGD with or without imiquimod in combination of phototherapy and anti-PD-1 checkpoint blockade antibody. Two treatment cycles were applied, and phototherapy was only induced repeatedly on one tumor.

Magnetic Resonance Imaging (MRI)

Following at least 21 days of age, transgenic FVB mice with spontaneous bladder cancer were treated for three weeks with the triple combinational treatment of PLZ4-ICG-Imiq + laser + anti PD-1, along with control mice receiving no treatment. These mice were anesthetized and underwent bladder imaging via MRI on a weekly basis to monitor the progression of mass size until the end of their lifespan. Bladder mass volume was calculated from T2 sliced images using AMIRA software.

1.4. RESULTS AND DISCUSSION

Biodistribution

The PLZ4-ICGD-Imiq nanoparticle exhibited targeted specificity to the bladder (tumor) as soon as 6 hours following intravenous administration, with peak fluorescence observed between 24 to 48 hours (Fig. 5). ICGD accumulation was found in all organ tissues studies, including the heart, liver, spleen, lung, kidney, bladder (tumor), and

skin. After 24 hours, minimal to no presence of PLZ4-ICGD-Imiq was observed in the heart, lung, and spleen tissues, which indicates lower risk of adverse effects or toxicity related to these organs. The liver and bladder (tumor) were the major depots of nanoparticle accumulation, yet ICGD fluorescence declined steadily over the 120-hour period, approaching complete excretion. After the bladder tumor was homogenized, ICGD concentrations were measured and shown in Figure 5. At the 24-hour mark, there was a peak average accumulation of ICGD detected in the tissue of around 0.7 µg/g, notably higher than the concentration values seen compared to other time points. Based on these results, a time point of 24 hours post i.v. was chosen for the photodynamic therapy treatment.

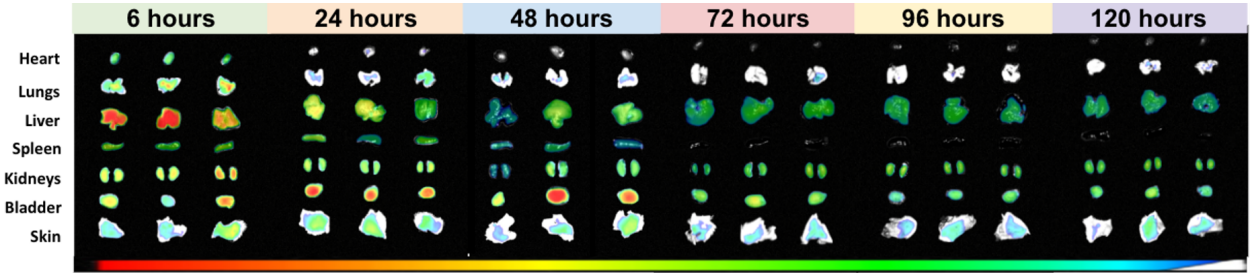

Figure 5: Biodistribution of PLZ4-ICGD-Imiquimod NPs in mice bearing spontaneous bladder cancer. Organs were removed 6, 24, 48, 72, 96, and 120 hrs after i.v. injection. In vivo imaging system (IVIS) was used to measure the fluorescence intensity of ICGD found in the heart, lungs, liver, spleen, kidneys, bladder (tumor), and skin. The color scale at the bottom indicates fluorescent intensity.

Determining the single dose toxicity from hematologic analysis

Commonly used for immunotherapy, topical Imiquimod binds agonistically to TLR-7 in order to enhance the innate and adaptive immune system on their antitumor and antiviral effects[9], which led to its approval by the US Food and Drug Administration[7]. Its approved indications include the treatment of external anogenital warts, superficial basal cell carcinoma, actinic keratoses, and skin lesions associated

with human papillomavirus (HPV) and UV exposure.[14] Currently, imiquimod's approval is limited to the localized treatment of basal cell carcinoma and other topical uses due to its toxicity upon systemic administration.[17] However, we hypothesize that through the packaging of imiquimod into a nanoformulated micelle, intravenous administration can be successfully achieved with significantly lower toxicity. Therefore, PLZ4-ICGD-Imiq would be able to successfully be taken up at its targeted tumor site in the bladder, as well as other metastatic areas. FVB mice were used to determine the toxicities and optimal PLZ4-ICGD-Imiquimod dose suitable for photodynamic therapy. Following a single dose of the nanoparticle on Day 1 and photodynamic therapy on Day 2, it was observed that mice experienced a dose-dependent increase in cholesterol, triglycerides, and alkaline phosphatase levels by Day 3. Because hyperlipidemia can typically indicate cardiovascular or kidney damage and elevated alkaline phosphatase is linked with liver or bone damage, blood toxicity was further observed after days 10 and 17. All measured parameters across all tested doses returned within normal female FVB ranges. All other CMP parameters were within normal ranges on days 3, 10, and 17 for all dose groups (Fig. 6, Tables #1-6).

PLZ4-ICGD:Imiq/kg

Normal Low Range | 50mg:1.25mg | 100mg:2.5mg | 200mg:5mg

Control | 75mg:1.875mg | 150mg:3.75mg | Normal High Range

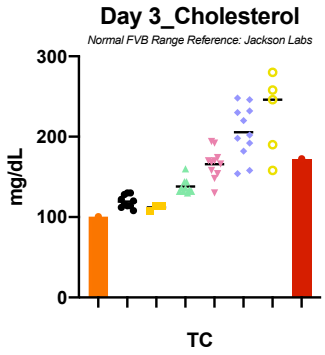

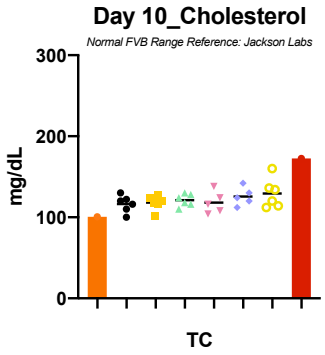

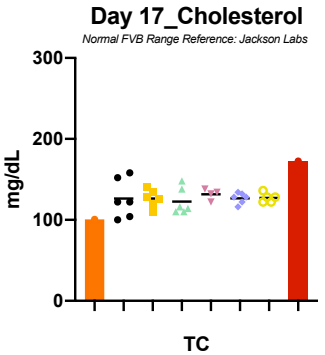

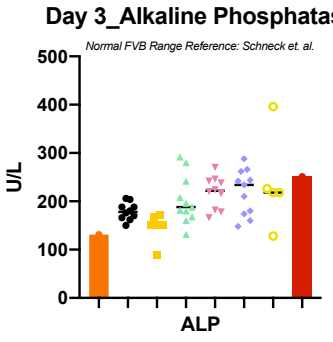

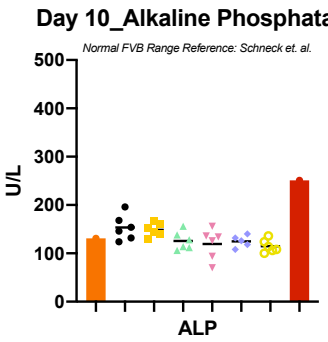

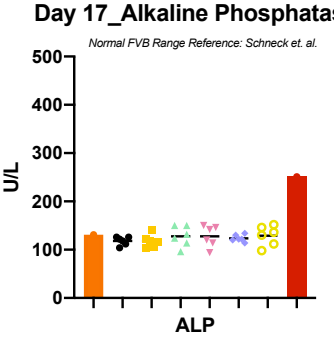

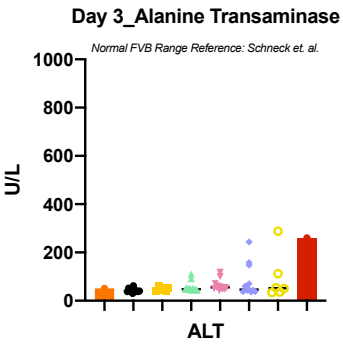

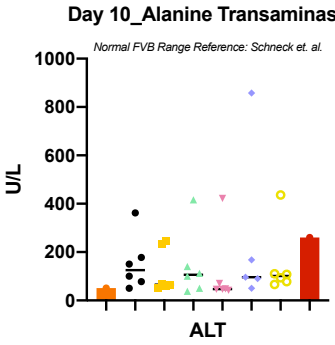

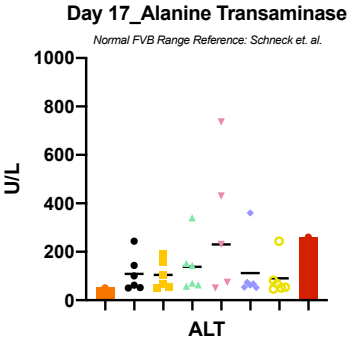

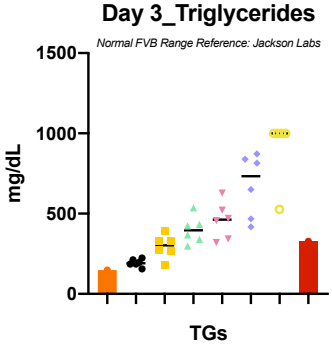

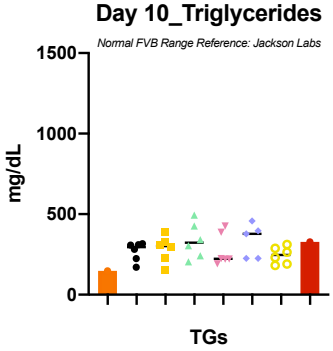

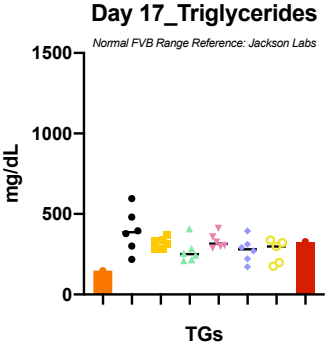

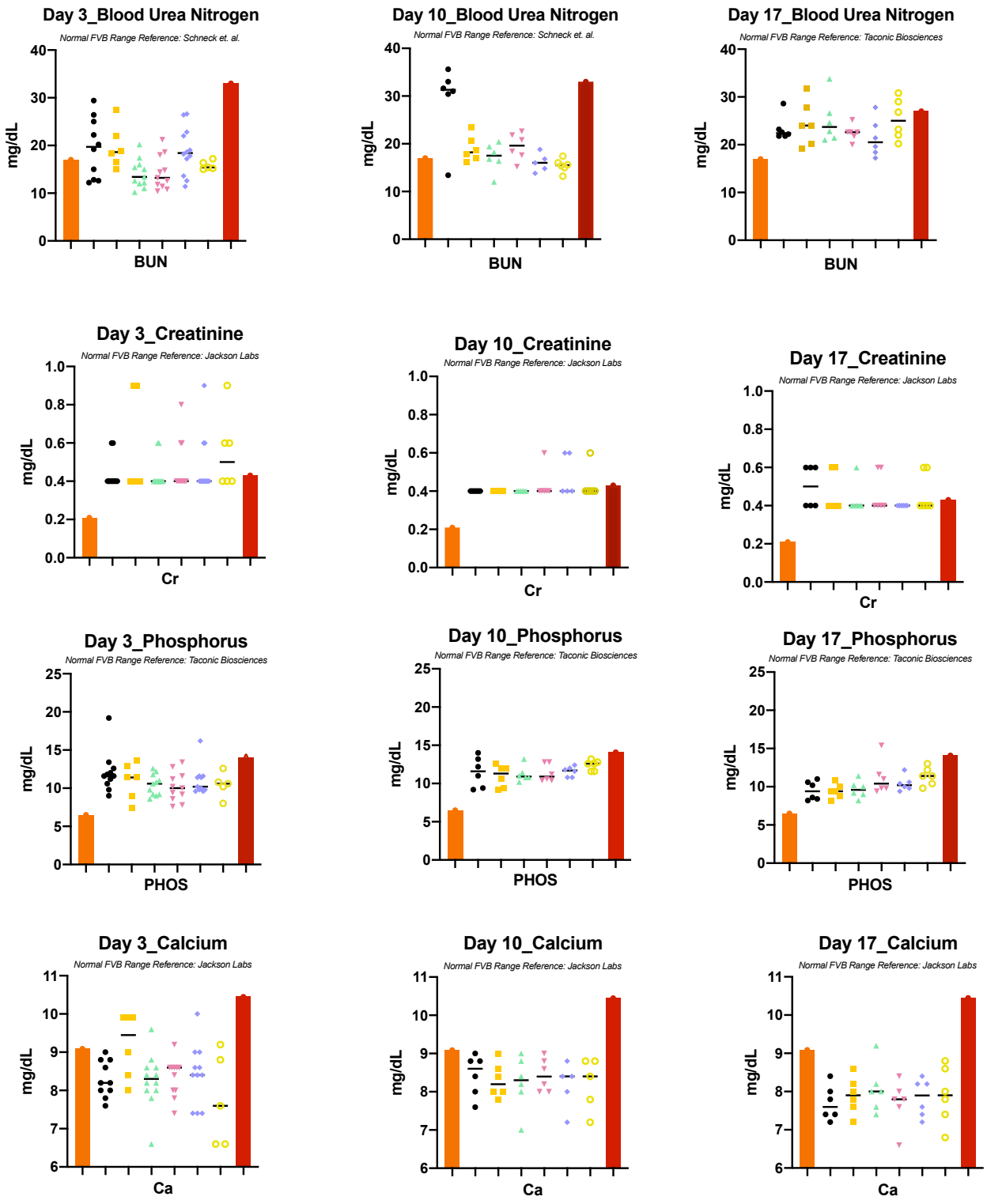

Figure 6: Hematology values of female FVB mice injected with various indicated doses of PLZ4-ICGD-Imiq. The first and last column (orange and red, respectively) are the minimum and maximum average normal female FVB range based on references from Jackson Labs, Schneck et. al., or Taconic Biosciences. The color key is shown at the top.

Table 1. Blood chemistry of expanded single dose acute toxicity study in FVB mice (day 3)

		Group						*Female FVB Range References (95% CI)*		
Parameter	**Unit**	**Ctrl (0mg/0mg)**	**PCNP/Imiq (50mg/1.25mg)**	**PCNP/Imiq (75mg/1.875mg)**	**PCNP/Imiq (100mg/2.5mg)**	**PCNP/Imiq (150mg/3.75mg)**	**PCNP/Imiq (200mg/5mg)**	**Jackson Labs**	**Taconic**	**Schneck et.al.**
BUN	**mg/dL**	19.50	20.60	14.13	14.29	18.49	15.84	15.46-21.14	11-27	17-33
Creatinine	**mg/dL**	0.44	0.57	0.44	0.44	0.44	0.48	0.21-0.43	0.1	0.12-0.28
Phosphorus	**mg/dL**	11.36	10.95	10.44	10.16	11.02	10.44	7.46-11.14	6.5-14.1	N/A
Calcium	**mg/dL**	8.30	8.47	8.42	8.35	8.42	8.53	9.09-10.45	10.1-11.3	N/A
Total Protein	**g/dL**	5.34	5.90	5.64	5.18	5.73	8.88	5.02-5.82	5.2-6.0	N/A
Albumin	**g/dL**	2.56	2.76	2.64	2.71	2.71	5.52	3.12-3.52	N/A	N/A
Globulin	**g/dL**	2.78	3.44	3.00	2.47	3.02	3.36	N/A	N/A	N/A
Glucose	**mg/dL**	146.20	102.67	138.91	134.36	145.64	133.60	103.4-172.6	116-196	N/A
Cholesterol	**mg/dL**	119.40	112.00	141.27	165.82	205.64	226.40	100.72-139.28	N/A	N/A
ALT (GPT)	**U/L**	41.80	49.00	58.00	59.45	84.18	57.20	31.2-58.8	0-149	N/A
ALP	**U/L**	179.00	146.17	202.55	261.64	218.91	237.20	65.4-108.2	N/A	115-251
GGT	**U/L**	< 10	< 10	< 10	< 10	< 10	578.00	< 10	N/A	N/A
Total Bilirubin	**mg/dL**	0.34	0.68	0.65	0.51	0.85	9.48	0.31-0.59	0.1	N/A
Triglycerides	**mg/dL**	193.33	296.17	399.67	456.33	677.17	>1000	148-328	N/A	N/A

Table 2. CMP of expanded single dose acute toxicity study in FVB mice (day 10)

		Group						*Female FVB Range References (95% CI)*		
Parameter	**Unit**	**Ctrl (0mg/0mg)**	**PCNP/Imiq (50mg/1.25mg)**	**PCNP/Imiq (75mg/1.875mg)**	**PCNP/Imiq (100mg/2.5mg)**	**PCNP/Imiq (150mg/3.75mg)**	**PCNP/Imiq (200mg/5mg)**	**Jackson Labs**	**Taconic**	**Schneck et.al.**
BUN	**mg/dL**	29.17	18.93	17.20	19.40	15.73	15.43	15.46-21.14	11-27	17-33
Creatinine	**mg/dL**	0.40	0.40	0.40	0.43	0.50	0.43	0.21-0.43	0.1	0.12-0.28
Phosphorus	**mg/dL**	11.50	10.97	11.23	11.37	11.57	12.40	7.46-11.14	6.5-14.1	N/A
Calcium	**mg/dL**	8.43	8.30	8.23	8.43	8.16	8.20	9.09-10.45	10.1-11.3	N/A
Total Protein	**g/dL**	5.80	5.57	6.03	5.63	6.10	6.77	5.02-5.82	5.2-6.0	N/A
Albumin	**g/dL**	2.70	2.57	2.83	2.53	3.00	3.70	3.12-3.52	N/A	N/A
Globulin	**g/dL**	3.10	3.00	3.20	3.10	3.10	3.07	N/A	N/A	N/A
Glucose	**mg/dL**	143.33	143.67	134.67	143.33	159.33	164.67	103.4-172.6	116-196	N/A
Cholesterol	**mg/dL**	116.33	118.00	121.00	118.00	123.67	129.33	100.72-139.28	N/A	N/A
ALT (GPT)	**U/L**	153.00	120.00	142.67	112.33	476.67	148.67	31.2-58.8	0-149	N/A
ALP	**U/L**	153.33	148.67	125.67	119.33	123.00	114.67	65.4-108.2	N/A	115-251
GGT	**U/L**	50.00	< 10	< 10	< 10	94.00	160.67	< 10	N/A	N/A
Total Bilirubin	**mg/dL**	1.50	0.67	1.47	0.93	2.20	3.80	0.31-0.59	0.1	N/A
Triglycerides	**mg/dL**	268.33	283.67	335.33	278.67	351.00	244.33	148-328	N/A	N/A

Table 3. CMP of expanded single dose acute toxicity study in FVB mice (day 17)

		Group						*Female FVB Range References (95% CI)*		
Parameter	**Unit**	**Ctrl (0mg/0mg)**	**PCNP/Imiq (50mg/1.25mg)**	**PCNP/Imiq (75mg/1.875mg)**	**PCNP/Imiq (100mg/2.5mg)**	**PCNP/Imiq (150mg/3.75mg)**	**PCNP/Imiq 200mg/5mg)**	**Jackson Labs**	**Taconic**	**Schneck et.al.**
BUN	**mg/dL**	23.37	24.50	25.03	22.47	21.40	25.33	15.46-21.14	27-Nov	17-33
Creatinine	**mg/dL**	0.50	0.47	0.43	0.47	0.40	0.47	0.21-0.43	0.1	0.12-0.28
Phosphorus	**mg/dL**	9.50	9.43	9.67	11.17	10.40	11.37	7.46-11.14	6.5-14.1	N/A
Calcium	**mg/dL**	7.70	7.90	8.07	7.70	7.83	7.90	9.09-10.45	10.1-11.3	N/A
Total Protein	**g/dL**	5.50	5.37	5.27	5.60	5.33	5.27	5.02-5.82	5.2-6.0	N/A
Albumin	**g/dL**	2.67	2.53	2.50	2.77	2.53	2.67	3.12-3.52	N/A	N/A
Globulin	**g/dL**	2.83	2.83	2.77	2.83	2.80	2.60	N/A	N/A	N/A
Glucose	**mg/dL**	173.00	153.00	196.00	179.00	164.67	199.33	103.4-172.6	116-196	N/A
Cholesterol	**mg/dL**	131.60	126.33	122.67	131.50	126.67	127.20	100.72-139.28	N/A	N/A
ALT (GPT)	**U/L**	108.67	104.33	138.00	422.67	111.67	90.67	31.2-58.8	0-149	N/A
ALP	**U/L**	118.00	117.67	127.67	127.67	123.67	129.00	65.4-108.2	N/A	115-251
GGT	**U/L**	< 10	< 10	< 10	< 10	< 10	< 10	< 10	N/A	N/A
Total Bilirubin	**mg/dL**	1.10	0.93	0.63	1.53	0.70	1.13	0.31-0.59	0.1	N/A
Triglycerides	**mg/dL**	394.67	319.67	270.00	330.67	277.00	222.00	148-328	N/A	N/A

Table 4. CMP of expanded single dose acute toxicity study in FVB mice (day 3)

		Group						*Female FVB Range References (95% CI)*		
Parameter	**Unit**	**Ctrl (0mg/0mg)**	**PCNP/Imiq (50mg/1.25mg)**	**PCNP/Imiq (75mg/1.875mg)**	**PCNP/Imiq (100mg/2.5mg)**	**PCNP/Imiq (150mg/3.75mg)**	**PCNP/Imiq (200mg/5mg)**	**Jackson Labs**	**Taconic**	**Schneck et.al.**
WBC	**10^3 cells/µL**	5.17	6.12	4.88	5.94	5.44	6.23	2.94-10.82	2.23-11.71	17-33
LYM	**10^3 cells/µL**	4.41	5.25	4.07	4.70	4.36	5.08	1.00-4.92	2.03-10.21	0.12-0.28
MONO	**10^3 cells/µL**	0.31	0.38	0.29	0.44	0.39	0.43	0-0.08	0-0.39	N/A
GRAN	**10^3 cells/µL**	0.44	0.48	0.52	0.80	0.70	0.73	N/A	N/A	N/A
LYM %	**%**	85.03	86.02	83.43	79.17	81.12	81.28	73-91	N/A	N/A
MONO %	**%**	5.36	5.53	5.40	6.31	5.62	5.35	0.51-1.63	N/A	N/A
GRAN %	**%**	9.61	8.45	11.17	14.52	13.26	13.38	N/A	N/A	N/A
HCT	**%**	38.46	40.38	37.02	41.46	37.87	37.60	40.22-47.78	46-54.8	N/A
MCV	**fL**	50.56	50.70	50.84	50.14	51.32	51.10	43.62-46.18	49-53	N/A
RDWa		32.47	32.67	32.64	32.54	33.51	32.95	N/A	N/A	N/A
RDW %	**%**	17.39	17.35	17.21	17.53	17.41	17.33	12.48-19.12	N/A	115-251
HGB	**g/dL**	12.00	12.60	11.61	13.09	12.22	12.38	14.2-16.2	14.2-17	N/A
MCHC	**g/dL**	31.27	31.23	31.80	31.67	32.38	33.23	33.48-35.52	30.2-31.8	N/A
MCH	**pg**	15.79	15.85	16.14	15.88	16.61	16.95	15.28-15.72	15.4-16.2	N/A
RBC	**10^6 cells/µL**	7.61	7.96	7.26	8.27	7.38	7.35	9.18-10.42	9.01-10.77	17-33
PLT	**10^3 cells/µL**	327.29	406.83	359.33	328.33	392.67	415.75	450-1178	1248-1984	0.12-0.28
MPV	**fL**	6.21	6.33	6.44	6.14	6.10	6.03	1.48-8.36	N/A	N/A

Table 5. CBC of expanded single dose acute toxicity study in FVB mice (day 10)

		Group						*Female FVB Range References (95% CI)*		
Parameter	**Unit**	**Ctrl (0mg/0mg)**	**PCNP/Imiq (50mg/1.25mg)**	**PCNP/Imiq (75mg/1.875mg)**	**PCNP/Imiq (100mg/2.5mg)**	**PCNP/Imiq (150mg/3.75mg)**	**PCNP/Imiq (200mg/5mg)**	**Jackson Labs**	**Taconic**	**Schneck et.al.**
WBC	**10^3 cells/µL**	7.73	7.90	8.06	7.70	8.60	6.25	2.94-10.82	2.23-11.71	17-33
LYM	**10^3 cells/µL**	6.32	6.57	6.63	6.13	6.90	5.12	1.00-4.92	2.03-10.21	0.12-0.28
MONO	**10^3 cells/µL**	0.50	0.45	0.53	0.50	0.62	0.40	0-0.08	0-0.39	N/A
GRAN	**10^3 cells/µL**	0.92	0.88	0.90	1.07	1.08	0.73	N/A	N/A	N/A
LYM %	**%**	81.55	82.70	81.93	79.07	79.88	81.57	73-91	N/A	N/A
MONO %	**%**	6.28	5.23	5.94	5.65	6.40	5.45	0.51-1.63	N/A	N/A
GRAN %	**%**	12.17	12.07	12.13	15.28	13.72	12.98	N/A	N/A	N/A
HCT	**%**	42.02	38.65	40.19	41.65	41.57	37.78	40.22-47.78	46-54.8	N/A
MCV	**fL**	51.38	49.67	49.37	50.32	49.63	48.57	43.62-46.18	49-53	N/A
RDWa		35.32	31.78	31.60	32.42	31.70	30.35	N/A	N/A	N/A
RDW %	**%**	17.95	17.38	17.30	17.15	17.13	16.98	12.48-19.12	N/A	115-251
HGB	**g/dL**	12.52	12.12	12.59	12.87	13.07	12.08	14.2-16.2	14.2-17	N/A
MCHC	**g/dL**	29.85	31.48	31.27	30.95	31.48	32.13	33.48-35.52	30.2-31.8	N/A
MCH	**pg**	15.30	15.63	15.47	15.57	15.63	15.62	15.28-15.72	15.4-16.2	N/A
RBC	**10^6 cells/µL**	8.18	7.78	8.13	8.28	8.37	7.78	9.18-10.42	9.01-10.77	17-33
PLT	**10^3 cells/µL**	347.83	363.17	365.00	354.00	393.17	3.45.67	450-1178	1248-1984	0.12-0.28
MPV	**fL**	5.75	5.83	5.84	5.47	5.75	5.75	1.48-8.36	N/A	N/A

Table 6. CBC of expanded single dose acute toxicity study in FVB mice (day 17)

		Group						*Female FVB Range References (95% CI)*		
Parameter	**Unit**	**Ctrl (0mg/0mg)**	**PCNP/Imiq (50mg/1.25mg)**	**PCNP/Imiq (75mg/1.875mg)**	**PCNP/Imiq (100mg/2.5mg)**	**PCNP/Imiq (150mg/3.75mg)**	**PCNP/Imiq (200mg/5mg)**	**Jackson Labs**	**Taconic**	**Schneck et.al.**
WBC	**10^3 cells/µL**	5.10	5.53	5.15	6.40	7.92	6.08	2.94-10.82	2.23-11.71	17-33
LYM	**10^3 cells/µL**	4.20	4.53	4.20	5.28	6.68	5.00	1.00-4.92	2.03-10.21	0.12-0.28
MONO	**10^3 cells/µL**	0.35	0.37	0.33	0.33	0.42	0.40	0-0.08	0-0.39	N/A
GRAN	**10^3 cells/µL**	0.55	0.63	0.62	0.78	0.82	0.68	N/A	N/A	N/A
LYM %	**%**	81.85	81.57	81.40	82.70	84.32	81.52	73-91	N/A	N/A
MONO %	**%**	6.62	5.70	5.88	5.17	5.15	5.67	0.51-1.63	N/A	N/A
GRAN %	**%**	11.53	12.73	12.72	12.13	10.53	12.82	N/A	N/A	N/A
HCT	**%**	39.67	39.92	41.07	38.05	41.07	37.25	40.22-47.78	46-54.8	N/A
MCV	**fL**	49.17	49.15	49.17	49.42	49.17	49.28	43.62-46.18	49-53	N/A
RDWa		31.03	31.13	31.40	30.98	31.48	31.53	N/A	N/A	N/A
RDW %	**%**	17.00	17.10	17.23	16.93	17.40	17.43	12.48-19.12	N/A	115-251
HGB	**g/dL**	12.38	12.43	12.70	11.78	12.67	11.63	14.2-16.2	14.2-17	N/A
MCHC	**g/dL**	31.37	31.18	30.95	31.12	30.93	31.25	33.48-35.52	30.2-31.8	N/A
MCH	**pg**	15.43	15.32	15.23	15.33	15.20	15.40	15.28-15.72	15.4-16.2	N/A
RBC	**10^6 cells/µL**	8.06	8.12	8.35	7.70	8.34	7.56	9.18-10.42	9.01-10.77	17-33
PLT	**10^3 cells/µL**	348.83	378.17	370.67	394.83	394.33	438.50	450-1178	1248-1984	0.12-0.28
MPV	**fL**	5.58	5.63	5.65	5.78	5.78	5.88	1.48-8.36	N/A	N/A

Transgenic Survival Study

For this study, we utilized the UPII-Ras* and UPII-SV40T double transgenic mice, chosen due to their rapid development of spontaneous localized bladder cancer within one month after birth and typically die from urinary obstruction within 5 weeks. Treatment began between 21-27 days of age, and three cycles of treatment was completed over the course of three weeks: the nanoparticle was administered intravenously on day 1, phototherapy was performed on day 2, and anti PD-1 was administered intraperitoneally on day 3. On average, control mice that received no treatment had a median survival of 40 days, while the mice that only received Anti PD-1 had a median survival of 42 days. Anti PD-1 treated mice showed no significant difference compared to the control ($P = 0.3542$). Phototherapy alone significantly extended the median survival to 72 days ($P = 0.0006$) by damaging tumor blood vessels and tumor cells with heat,[25] presumably disrupting blood flow crucial for continued growth. The mice that received PLZ4-ICGD + Laser or PLZ4-ICGD + Laser + Anti PD-1 had similar median survival at 79.5 days and 73 days, respectively. The longest median survival was in the mice that received the triple combination of PLZ4-ICGD-Imiq + Laser + Anti PD-1 ($P < 0.001$) with the median survival of 94 days, with several mice living past 150 days. Within the time period that was monitored, there was no significant disparity in lifespan or adverse toxicity seen between the control mice and those treated solely with the PLZ4-ICGD polymer ($P = 0.0503$). Similarly, no significant difference was observed in the lifespan between the control mice and PLZ4-ICGD-Imiq treatment group ($P = 0.1171$), suggesting the safety of chosen imiquimod dosage during the observed period. However, further studies need to be conducted on healthy mice in order to see the long-term effect of this drug. In conclusion, the data presented in Figure 7 distinctly

illustrates the life-prolonging advantages of the triple combination therapy involving the nanoparticle, phototherapy, and checkpoint blockade treatment compared to the untreated control mice with double transgenic bladder tumors. Statistical significance was calculated using the Log-Rank (Mantel-Cox) test, and the multiple comparison threshold was adjusted using a Bonferroni-corrected α value of 0.00625.

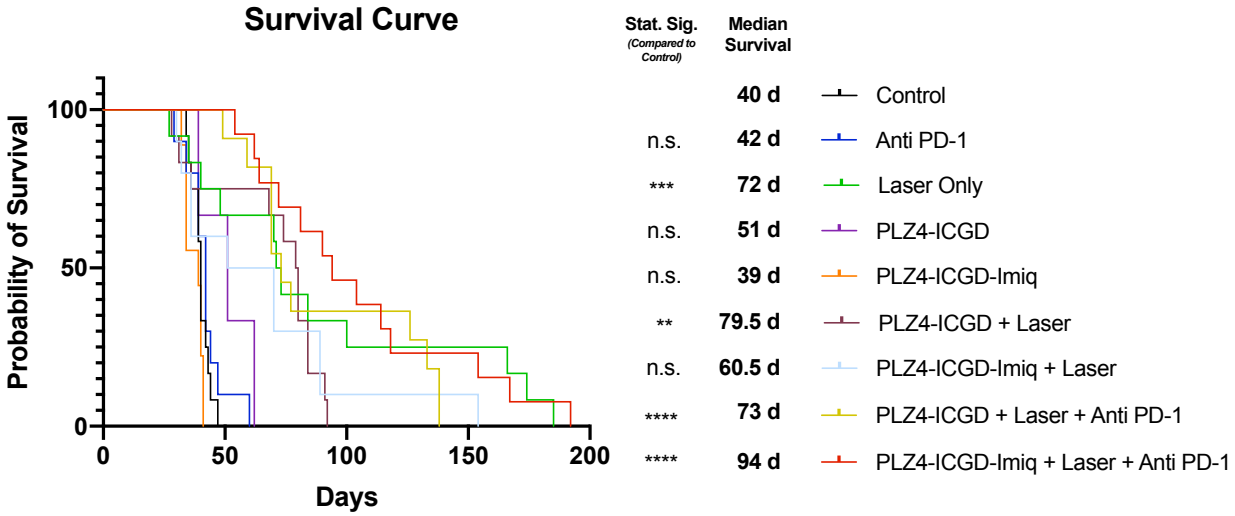

Figure 7: Kaplan-Meier survival curves computed for FVB transgenic mice with urothelial cell carcinoma. Treatment groups included untreated control mice (n=12), anti PD-1 only treatment (n=10), Laser only treatment (n=12), PLZ4-ICGD (n=3), PLZ4-ICGD-Imiquimod (n=9), PLZ4-ICGD + Laser (n=12), PLZ4-ICGD-Imiquimod + Laser (n=11), PLZ4-ICGD + Laser + Anti PD-1 (n=11), and PLZ4-ICGD-Imiquimod + Laser + Anti PD-1 (n=13).

Magnetic Resonance Imaging (MRI)

Following appropriate treatment, transgenic FVB mice bearing spontaneous bladder cancer were monitored via MRI for tumor mass progression on a weekly basis until death. Although the triple combinational therapy of PLZ4-ICGD-Imiq, phototherapy, and anti PD-1 significantly enhanced overall survival compared to untreated control mice, there was no significant decrease in bladder cancer mass over the course of treatment (Fig. 8). It is also notable that the overall bladder cavity in the triple treatment

group significantly increased, while the available space for urine volume significantly decreased. Based on these images, we observed the inner lining surrounding the lumen harbored healthy transitional epithelial cells, while the solid tumor cells surrounded the outer edges. Interestingly, in the mice depicted in Figure 8 the bladder volume (tumor) in the control group exhibited a significantly faster exponential increase by Day 46 compared to the treated mouse, which reached a similar tumor size around Day 81 of age.

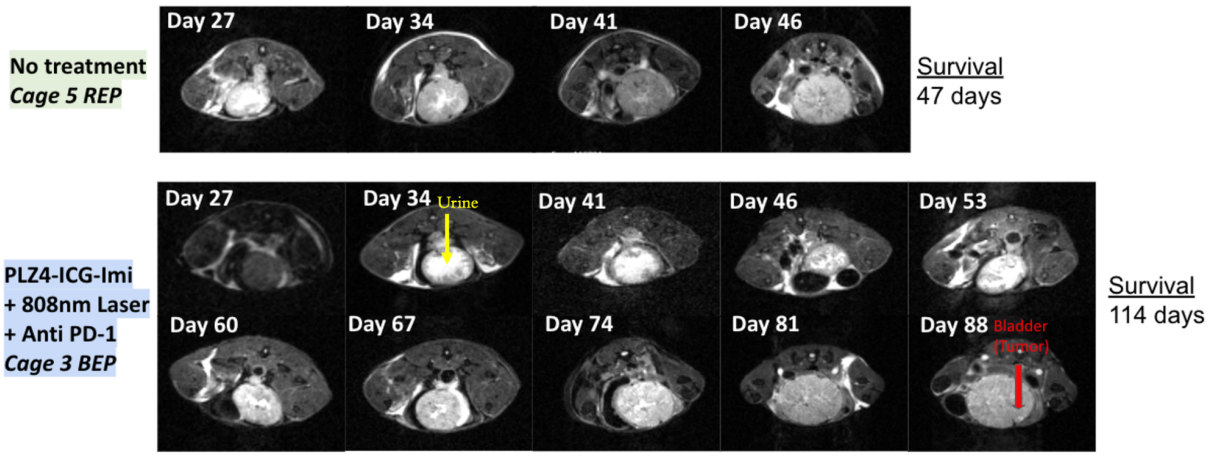

Figure 8: MRI image of mouse bladder emphasizing tumor progression over the course of the mouse lifespan. T2 images are shown here. The yellow arrow highlights white irregular areas to indicate the urine within the bladder. The red arrow highlights the darker solid mass of the tumor within the bladder. This untreated control mouse dies at 47 days, while the triple treated mouse died at age 114 days.

Anti-Tumor Efficacy Study in MB49 metastatic cancer mouse model

To assess the antitumor and systemic activity, we established bilateral subcutaneous mouse bladder cancer models using the carcinogen-inducing MB49-GFP labeled cells implanted in the left and right flanks. When tumors reached around 100 mm^3 in size, mice received treatments once a week for three weeks of either PBS, anti-

PD1, phototherapy alone, PLZ4-ICGD, PLZ4-ICGD + anti PD-1, PLZ4-ICGD-Imiq, or PLZ4-ICGD-Imiq + anti PD-1. With the exception of the PBS and anti-PD1 groups, all mice received weekly photodynamic therapy at 0.8 W/cm^2 for two minutes following 24 hours post i.v. treatment. At a wavelength of 808 nm, ICGD is activated by phototherapy and absorbs light to release heat as well as free radical and singlet oxygen, autonomously of oxygen.[26] This oxygen-independent property potentially enhances its efficacy in anaerobic conditions, such as within bladder tumor masses, relative to other photosensitizers.[27] Throughout each phototherapy session, we monitored the temperature rise specifically targeted at the primary tumor to ensure that ICGD effectively produced a robust photothermal effect and facilitated photochemical catalysis, leveraging its near-infrared absorption properties to generate increased ROS production. Under laser irradiation, the temperature of the tumor site in mice that were given our nano-formulation was found to reach up to 75.1 °C. After photothermal treatment, the tumor tissue in the mice showed obvious necrosis and reduced tumor area, proving that our nanoparticle has good photothermal effect (Fig. 9).

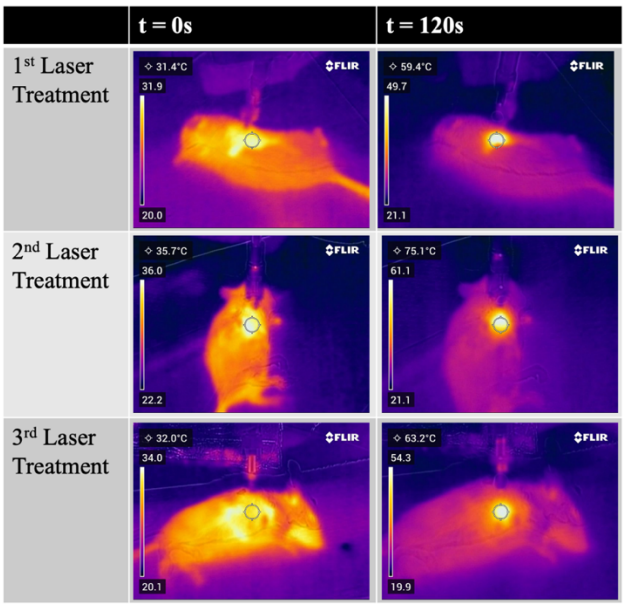

	Time (s)	Temperature (°C)
1st Laser Treatment	0	31.9
	30	40.5
	60	44.6
	90	48.2
	120	49.7
2nd Laser Treatment	0	35.7
	30	49.7
	60	57.8
	90	67.2
	120	75.1
3rd Laser Treatment	0	32.0
	30	44.7
	60	58.2
	90	61.7
	120	63.2
Average Temperature at 120s =		**62.67**

Figure 9: Photothermal images monitoring gradual temperature increase on primary tumor of a mouse receiving phototherapy from 808 nm laser at 0.78W/cm² for 2 minutes per treatment session.

Only one tumor (proximal) received light treatment, whereas the contralateral tumor (distal) was left untreated to represent a site of metastasis to determine the abscopal effect. Figure 10 represents the tumor growth trends between the proximal tumor and distal tumors in female albino C57BL/6 mice. While anti PD-1 treatment alone showed a moderate tumor volume reduction compared to the control, the triple treatment group of PLZ4-ICGD-Imiq + laser + anti PD-1 ($P < 0.0001$) and double treatment group of PLZ4-ICGD-Imiq + laser ($P = 0.0347$) significantly repressed tumor growth in the treated proximal sites. Remarkably, only the triple treatment group significantly reduced tumor volume in untreated distal tumor ($P < 0.0001$), compared to control mice. This data confirms that phototherapy applied to the “primary” tumor can trigger an abscopal effect against distant ("metastatic") tumors. Although both anti PD-1 and imiquimod immunomodulators are integral to the efficacy of triple-combination therapies with phototherapy, our results indicate that our nano-formulation incorporating

both imiquimod and i.p. anti-PD-1 are superior in eliciting an immune response compared to those containing imiquimod alone.

This study was repeated using male albino C57BL/6 mice to observe any sex-dependent discrepancies. At Day 19, compared with the control, the volumes of the proximal treated tumors were all reduced in PLZ4-ICGD (P=0.0039), PLZ4-ICGD + Anti PD-1 (P=0.0036), PLZ4-ICGD-Imiq (P=0.0099), and PLZ4-ICGD-Imiq + Anti PD-1 (P<0.0001) groups (Fig. 11). There was no significant reduction in the tumor volume between the control and anti PD-1 alone group (P=0.9511). To assess the systemic effect, tumor volumes of untreated distal sites were also measured. Interestingly, PLZ4-ICGD + anti PD-1 (P = 0.0005) and PLZ4-ICGD-Imiq + anti PD-1 (P=0.00017) groups showed significant reduction in tumor volume compared to the PBS control, while the remaining therapy groups showed no significant reduction (Fig. 11).

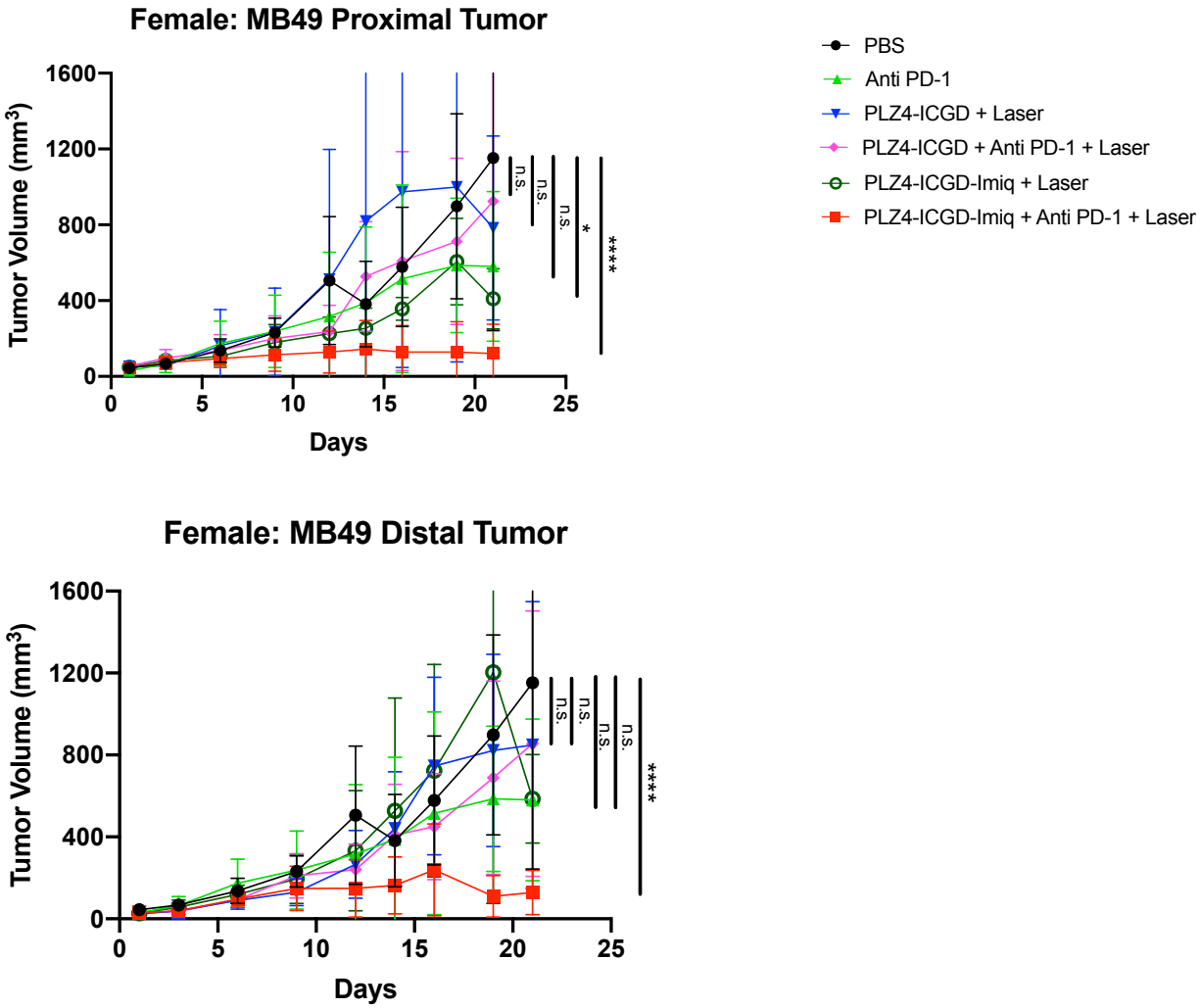

Figure 10: Using female C57BL/6 Albino mice, 5x10^5 MB49 cells were subcutaneously implanted on both flanks on day -5. On day 1, mice were treated with the nanoparticle with or without imiquimod at 1.875mg/kg via i.v. On day 2, mice received laser treatment, 0.8w/cm2 for 2 min, ICGD at 808nm. On day 3, mice received anti-PD1 antibodies at a concentration of 10mg/kg. This treatment was repeated on days 8,9,10. Primary (top graph) and distant (bottom graph) tumor volumes were observed between different groups (n=6 per group) over the course of treatment.

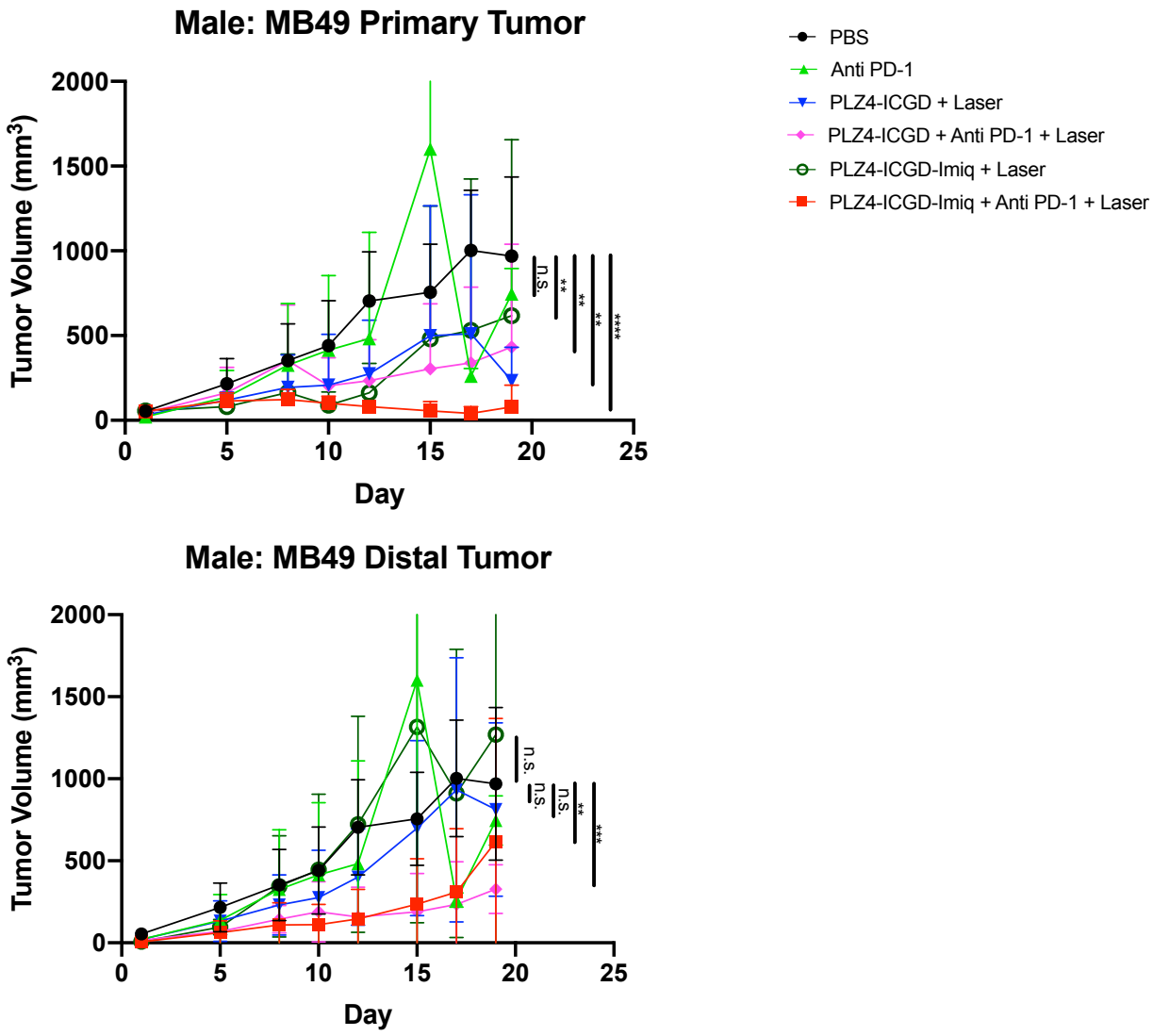

Figure 11: Using MALE C57BL/6 Albino mice, 5x10^5 MB49 cells were subcutaneously implanted on both flanks on Day -5. On day 1, mice were treated with the nanoparticle with or without imiquimod at 1.875mg/kg via i.v. On day 2, mice received laser treatment, 0.8w/cm2 for 2 min, ICGD at 808 nm. On day 3, mice received anti-PD1 antibodies at a concentration of 10 mg/kg. This treatment was repeated on days 8,9,10. Proximal (top graph) and distal (bottom graph) tumor volumes were observed between different groups (n=6 per group) over the course of treatment.

1.5. CONCLUSION

Among the prevalent malignancies globally, urothelial cell carcinoma has not witnessed advancements in treatment options and improvements in quality of life at the pace seen in other cancers, necessitating the urgent exploration of new alternatives to alleviate its burden.[15] Additionally, we have seen many mechanisms of resistance when treating bladder cancer and therefore the development of an improved and more effective therapy is critical. In this study we have developed a nanoparticle (PLZ4-ICGD-Imiquimod) that targets the overexpressed αvβ3 integrin found on human bladder cancer, capable of combination photo- and immuno- therapy.

The median survival for the mutant RAS and SV40 double transgenic FVB mice with bladder cancer was 40, 42 and 72 days for the control, anti-PD-1, and phototherapy alone, respectively, while the survival for the triple combination group is over 94 days. Longitudinal MRI was done to compare the bladder surface area within control mice and triple treatment therapy mice to determine tumor progression (Fig. 8). One observed control mouse died at Day 47, while the treated mouse survived until Day 114. However, it is important to note that the tumor volume of the triple treated mouse did not decrease over its lifespan. Phototherapy (PT) is conventionally regarded as a localized treatment. Nevertheless, when paired with immunotherapy, it can trigger abscopal anti-tumor responses, effectively reducing the growth of distal tumors (Fig. 10, 11). It suggests that PDT may induce immunogenic cell death, and it implies that combining PDT with immunotherapy can be a promising approach for the development of treatments for metastatic urothelial cell carcinoma.

While cytotoxic chemotherapy remains the established treatment for newly diagnosed bladder cancer with distant metastasis, immunotherapy serves as salvage

therapy or an option for patient's ineligible for chemotherapy or exhibiting PD-L1 expression. One significant strength of this project lies in the utilization of various clinically relevant animal models, including a transgenic model reflecting spontaneous bladder cancer development and the subcutaneous implantation of artificial MB49 cells, consistently demonstrating the enhanced effects of immunotherapy through PT. However, a potential limitation is the absence of human patient-derived bladder cancer samples with more complex somatic alterations in the cancer genomes. Humanized mice, created from immunocompromised strains, may exhibit substantial differences in their immune systems compared to both human patients and mouse models due to defects in thymus and lymphoid tissue.

In summary, the transgenic survival curve and anti-tumor efficacy study demonstrate that our targeted bladder cancer nanoparticle, PLZ4-ICGD-Imiquimod, combined with PT and anti-PD-1, shows significant promise for enhancing immunotherapy in locally advanced bladder cancer. It induces abscopal anti-tumor responses in untreated distant cancers, reduces metastasis, and prolongs survival compared to the negative single controls in each study. Future studies will be investigated on potential synergistic effects that may be attributed to multiple underlying mechanisms, such as PT-induced immunogenic cell death, the activation of dendritic cells through macromolecule modification, increased infiltration of immune cells into tumors, and alteration of the tumor immune microenvironment. These findings hold significant implications for the future management of bladder cancer, which has not seen clinical translation of survival in advanced cases of greater than 16 months.[16]

Chapter 2: Targeted Human Serum Albumin (HSA) Drug with Immunotherapy Against Breast Cancer

2.1. ABSTRACT

Breast cancer (BC) stands as one of the most prevalent malignancies globally, posing a significant threat to the health of the world population, particularly women, and contributing substantially to the global burden of disease.18 Our goal is to use precise site-specific ligation strategies to develop a novel targeting human serum albumin (HSA) conjugates for the enhancement in targeting of breast cancer. HSA is the most abundant protein in human blood plasma and plays a critical role in transportation of numerous drugs, metabolites, nutrients, and small molecules. Efforts have been made to use HSA as a covalent carrier for drug delivery, however none have been approved for clinical use. In this project, HSA covalently loaded with bortezomib (BTZ) will be site-specifically modified with two targeting ligands, LBF127 and LLP2A, to efficiently dual target breast cancer cells and activated natural killer (NK) cells. As a result, loaded BTZ will be delivered to the tumor microenvironment, and NK cells will be guided to the tumor cells for an enhanced immunotherapeutic effect.

2.2. INTRODUCTION

Breast cancer ranks as the most frequently diagnosed cancer in women, representing over one-tenth of new cancer cases annually, and stands as the second leading cause of cancer-related deaths among women globally.[19] Through site-specific ligation of HSA protein with targeting ligands, LBF127 and LLP2A, we expect to see this chemically-defined HSA conjugate to deliver Bortezomib (BTZ) to the tumor cells, and simultaneously have dual targeting effect to guide immune cells to the tumor

microenvironment for a synergistic anti-tumor effect. LBF127 is a membrane active peptide previously discovered in the Lam lab through screening one-bead one-compound combinatorial peptide library. It binds to fungal and mammalian giant unilamellar vesicles (GUVs), thereby mimicking fungal and mammalian membrane compositions.[20] We have found that LBF127 is able to preferentially bind to and taken up by breast cancer cell lines. However, the mechanism of cell uptake remains to be studied. LLP2A binds to activated α4β1 integrins present on activated NK cells and T-cells, which are necessary for a robust anti-cancer immune response.[21] Bortezomib is approved by FDA for the treatment liquid tumors, such as multiple myeloma or mantle cell lymphoma. However, there is limited data on the efficacy and safety of BTZ use in patients with solid tumors.[22] BTZ can be utilized for solid tumors in drug-resistant breast cancer cells for more successful treatments and reduced remission rates.[23] BTZ reversibly and selectively inhibits proteasomes that disrupts the ubiquitin proteasome pathway responsible for the degradation of numerous intracellular proteins.[22] Luna et al. demonstrated the dual effect of BTZ in enhancing NK cell susceptibility to cancer cells by targeting cancer stem-like cells (CSCs). BTZ upregulates the NK stress ligands MHC class I chain-related proteins A and B (MICA and MICB) on aldehyde dehydrogenase (ALDH)-positive CSCs, downregulates immune evasion molecules, and creates a synergistic effect that improves CSC elimination compared to either treatment alone.[31] Figure 12 depicts the mechanism of action in which HSA-LBF127-LLP2A-LYL1-BTZ dual targeting conjugate (labeled as HSA-2L) is administered into the bloodstream through i.v., where LLP2A can then bind to activated NK cells to guide them to the tumor site which is led by the interaction of LBF127 with the tumor cells. In this acidic

microenvironment, BTZ is released selectively to tumor cells, inducing apoptosis via the 26S proteasome, while also enhancing the expression of immune recognition molecules such as NKG2D and DNAM1 ligands, along with upregulating apoptosis-related receptors like DR3/DR4/DR5.[24] Therefore, there is an overall increase of the NK cell's tumor killing ability. Simultaneously, these NK cells will also increase interferon-gamma production to further activate additional NK cells for LLP2A to bind with.

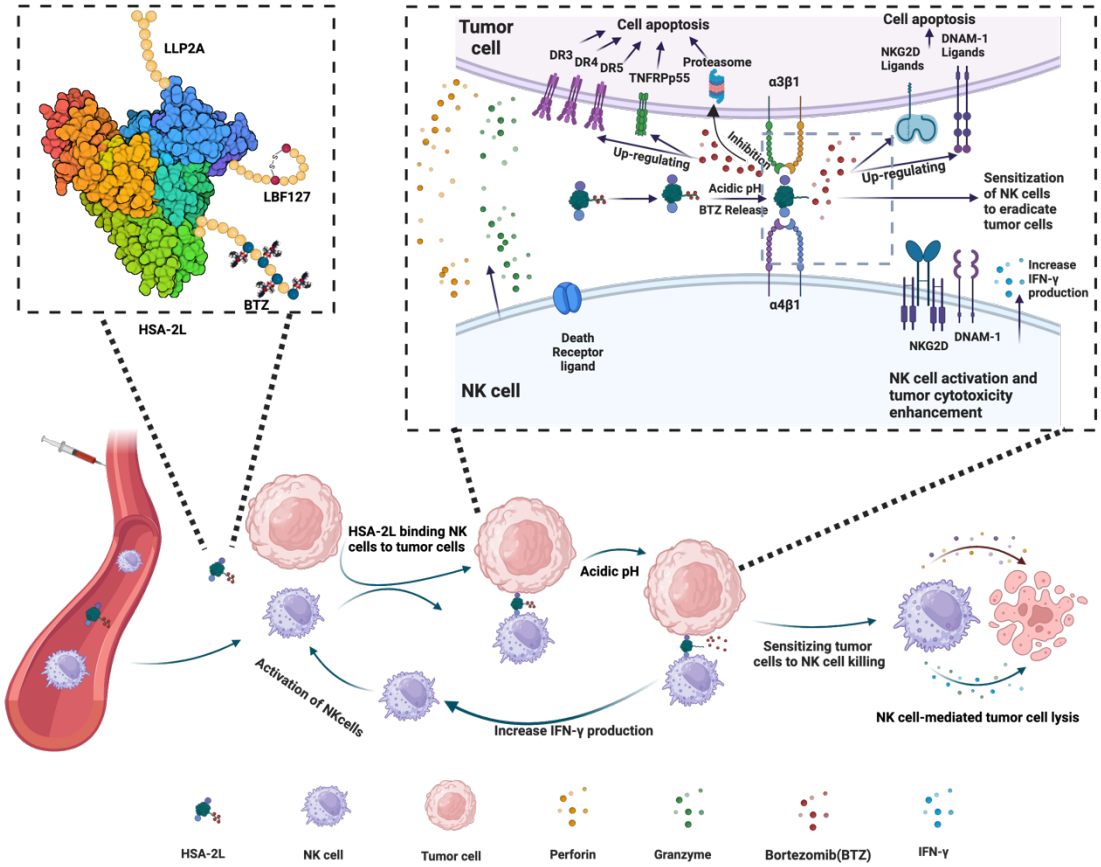

Figure 12: Cartoon schematic representing the mechanism of action of HSA-LBF127-LLP2A-LYL1-BTZ (labeled as HSA-2L-BTZ) when in contact with the tumor cell microenvironment.

2.3. MATERIALS AND METHODS

Cell-based Ligand Binding Assay

Cultured EO771 mouse breast cancer in Dulbecco's Modified Eagle Medium (DMEM) supplemented with 10% fetal bovine serum (FBS) and 1% Penicillin-Streptomycin at 37°C were grown at 1×10^4 cells/mL in 5% CO_2 was followed by 24 hr incubation. The cells were then incubated with PBS containing ligand-biotin for 30 minutes on ice. After unbound ligand-biotin was washed away with PBS, the cells were incubated with PBS containing Alexa Fluor™ 488 streptavidin for another 30 minutes on ice. Cells were finally fixed with 4% paraformaldehyde to maintain the shape of the cells and stained with DAPI.

Preparation of HSA-conjugates

HSA-conjugates were prepared by Dr. Junwei Zhao, post-doctoral fellow in the Lam lab. For HSA-LBF127-LLP2A-conjugate, LLP2A was attached to N-terminus Asp via Ugi reaction, and LBF127 was ligated to Cys34 via maleimide chemistry. For HSA-LXY30-LLP2A-conjugate, LXY30 was attached to N-terminus Asp via Ugi reaction and LLP2A was ligated to Cys34 via maleimide chemistry. For bortezomib covalent drug loading, the drug loading element LYL1-linker-$DOPA_4$ (DOPA = l-3,4-dihydroxyphenylalanine) was first site-specifically ligated to HSA via the reactive affinity element LYL1.[30] Then boron containing drugs such as bortezomib could be covalently loaded onto the drug loading element via specific interaction with the catechol side chain of DOPA by simply mixing the drug with HSA-conjugate in a 4:1 ratio.

MTS Cytotoxicity Assay

The cell proliferation, cell viability, and cytotoxicity of EO771 murine breast cancer cells was determined by the MTS assay. The cells were seeded in 96-well plates for 24 hours and exposed to various concentrations ranging from 5000 to 0.15 nM of BTZ in the following formulations: HSA-LBF127-BTZ + HSA-LBF127-LLP2A mixture, HSA-LBF127-BTZ, and BTZ alone. Equivalent concentration of BTZ mixed with HSA-LBF127-LLP2A and HSA alone devoid of drug loading element were also tested as negative controls. After being exposed to the HSA-conjugates and BTZ for 24 hours, the culture medium was removed from the plate and the cells were washed in PBS. MTS/PMS media solution (100μL) was mixed in each well with a final concentration of 333 μg/ml MTS and 25 μM PMS and incubated for an additional 2 hours. The absorbance of the formed formazan crystal was then measured at 490 nm using a plate reader. The half-maximal inhibitory concentration (IC50) 24 hour of HSA-BTZ-conjugates and BTZ alone was determined on the EO771 cell line by using the results of the MTS assay.

2.4. RESULTS AND DISCUSSION

In Vivo Study on BALB/c Mice using LXY30 Targeting Ligand

According to published findings, α3β1 integrin has emerged as a promising cancer biomarker and therapeutic target. As a result, the Lam lab has28 previously identified a cyclic nonapeptide known as LXY30 for the detection of α3β1 integrin on the surface of viable tumor cells. Furthermore, 4T1 murine breast cancer cells have been observed to exhibit overexpression of α3β1 integrin, promoting spontaneous metastasis.29 Therefore, we initially evaluated the anti-tumor efficacy of HSA-LXY30-

LLP2A-BTZ in BALB /c mice orthotopically implanted with 4T1 cells. After only three intravenous treatments, a significant reduction in tumor volume was observed in the HSA-LXY30-LLP2A-BTZ and HSA-LXY30-BTZ + HSA-LXY30-LLP2A combination groups compared to control groups receiving PBS or HSA alone (Fig. 13). However, immediately following the third treatment, all mice in the experimental groups, except for the PBS group, died. Autopsy findings suggested a potential allergic reaction to the HSA carrier, possibly causing over-proliferation of immune cells and cytokine storm, as evidenced by splenomegaly in all treated mice. Subsequent studies administering native HSA alone to BALB/c mice resulted in similar outcomes, indicating toxicity caused by HSA itself but not by conjugated ligands. The spleens from each group ranged between 440 – 606 mg, while the average spleen weight of BALB/c mice is around 62 mg.11 To further study the effect of HSA alone on BALB/c mice, HSA was administered via i.v. once and twice a week. Again, the mice died after the third injection, and autopsy showed enlarged spleens compared to the PBS control group (Fig. 14). Conversely, no toxicity was observed in all other tested mouse strains such as FVB, SCID, and C57BL/6. This confirms that native HSA is toxic to BALB/c mice, and we will need to switch to an alternative mouse strain such as C57BL/6 for future HSA drug delivery studies. EO771 is a luminal B subtype ERα-, ERβ +, PR+ and ErbB2+ mammary epithelial carcinoma cell line derived from a spontaneous breast cancer of a C57BL/6 mouse. Targeting ligand(s) against EO771 is therefore needed for this work.

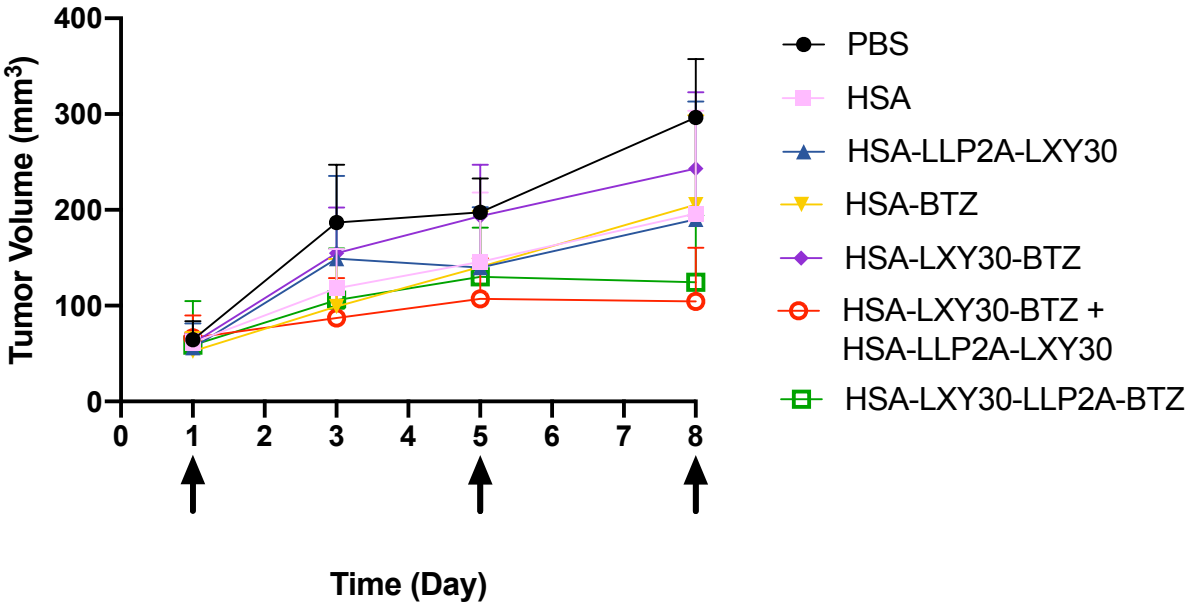

Figure 13: Tumor volume measurements of BALB/c mice orthotopically implanted with 4T1 cells. Arrows indicate the time of i.v. treatment. All groups, aside from PBS, died immediately following the 3rd dose.

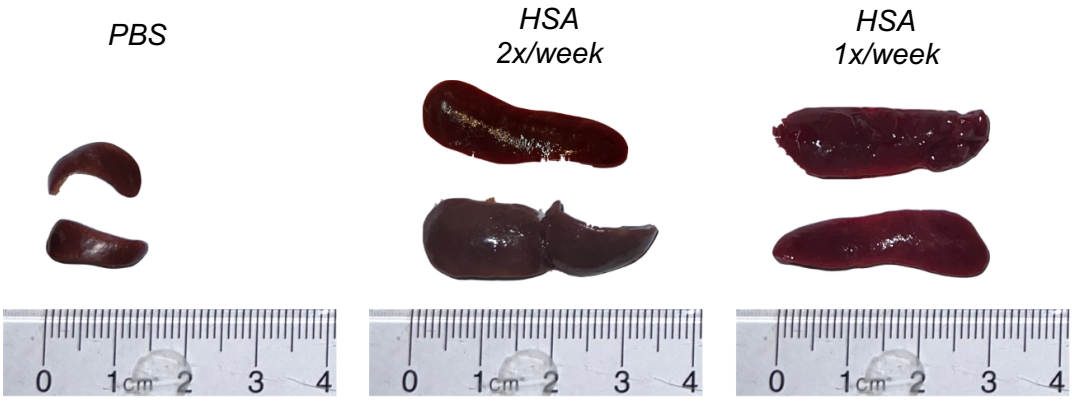

Figure 14: Autopsy of spleens from BALB/c mice treated with (a) PBS, (b) HSA - biweekly and (c) HSA – weekly. The treatment was observed over the course of three weeks.

Ligand-Biotin Binding Cell Assay

A number of biotinylated ligands are available in the Lam lab: a membrane active peptide LBF127, a αvβ3 integrin targeting peptide LXW7, three α3β1 integrin targeting peptides (LLY12, LLY13 and LXY30), and a α4β1 integrin targeting peptide LLP2A. To assess the binding of these peptides to EO771 cells, we first incubated the cells separately with each of these peptides for 30 min, washed, and followed by incubation with Alexa Fluor™ 488 streptavidin. DAPI was used to stain cell nuclei. AC-AEEA$_2$-Lys(Biotin)-Amide (AC = acetyl, AEEA = 2-(2-(2-aminoethoxy)ethoxy)acetic acid) peptide was served as the negative control. We found that of these selected ligands, LBF127 showed the strongest uptake by EO771 cells (Figure 15).

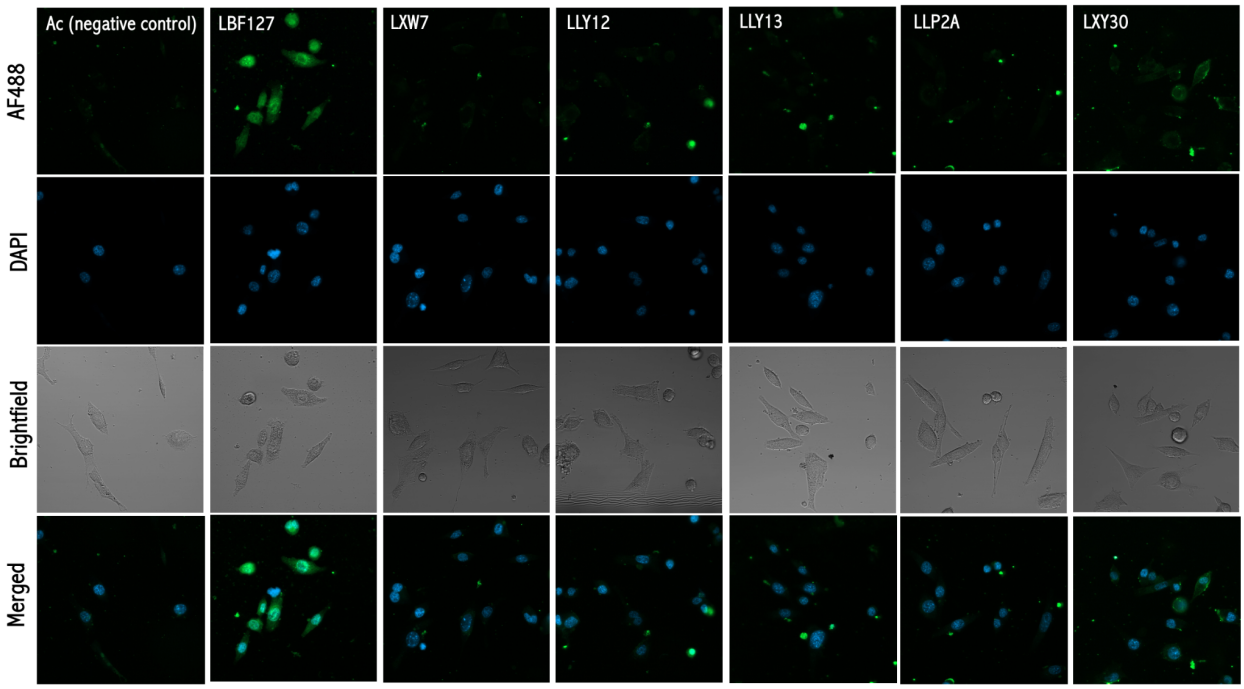

Figure 15: Fluorescence images of Ligand-Biotin Binding Screening Assay for EO771. 1 µL of ligand-Biotin was added to cells at a concentration of 1mM for 30 minutes over ice, followed by adding 2 µL of 1mg/mL of Alexa Fluor™ 488 streptavidin for 30 minutes over ice.

We then confirmed binding of our LBF127-specific nanoparticle to EO771 breast cancer cells by both optical and fluorescence microscopy. LBF127-biotin conjugation with Alexa Fluor™ 488 revealed significantly enhanced pseudo-green inside EO711 and MDA-MB-231 breast cancer cells after a one-hour incubation over lung carcinoma (A549), cholangiocarcinoma (SB1), and bladder carcinoma (T24). Pseudo-blue from of cell nuclei from DAPI staining (ex./em. At 359/456 nm) are also shown in Figure 16. This data therefore supports our notion that LBF127 peptide binding specificity to breast cancer cell lines over other cancer cell lines.

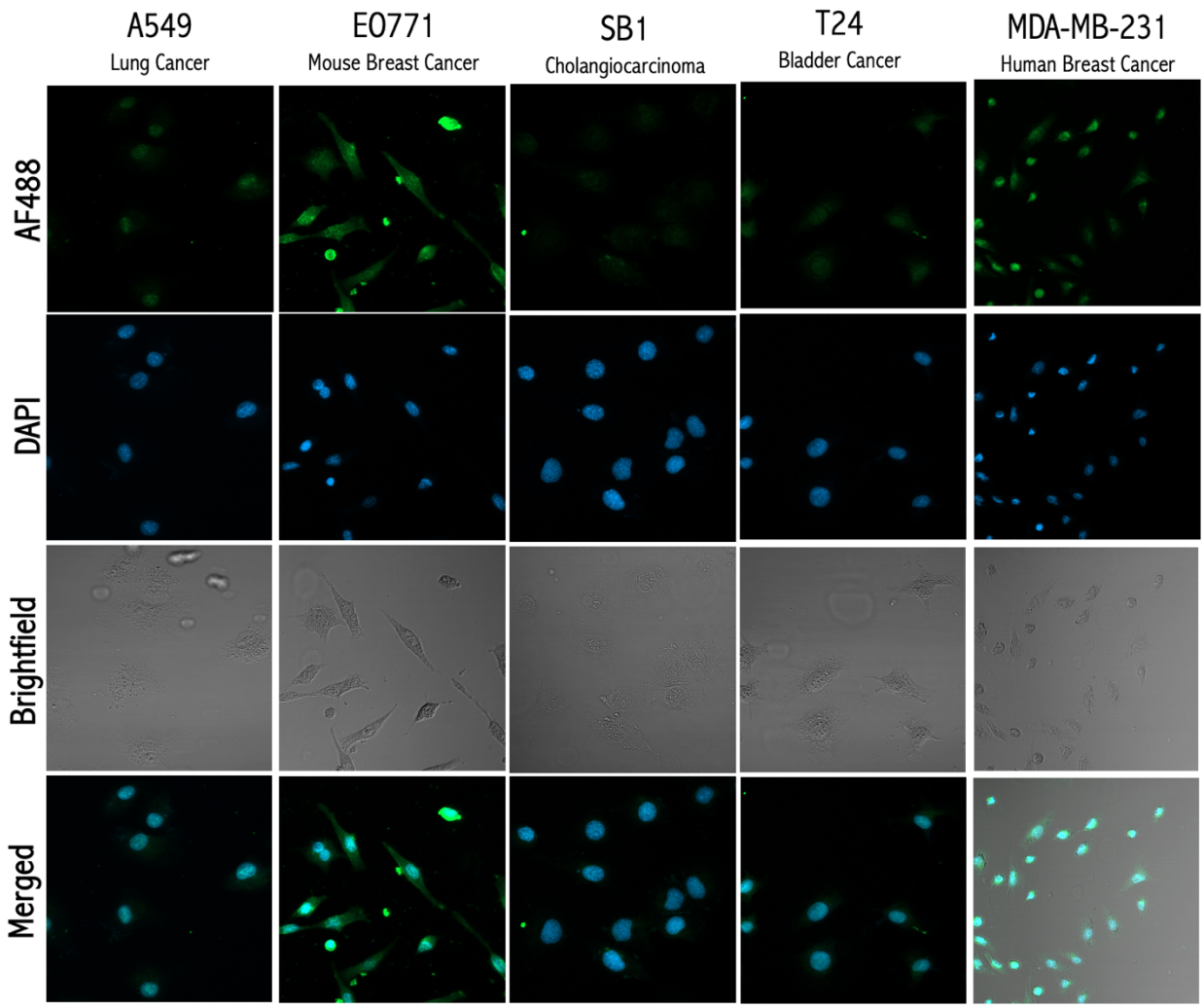

Figure 16: LBF127-Biotin Cell Binding Specificity Assay comparing various cancer cell lines. 1 µL of ligand-Biotin was added to cells at a concentration of 1mM LBF127 for 30 minutes over ice, followed by adding 2 µL of 1mg/mL of Alexa Fluor™ 488 for 30 minutes over ice.

Nanoparticle Cellular Uptake Assay

EO771 cells were cultured and treated in vitro with four HSA-conjugates with ICGD-boronate covalently loaded onto the drug loading affinity element, alongside a control of free indocyanine green derivative (ICGD) alone used for fluorescent tracking: HSA-LBF127-LLP2A-ICGD, HSA-LBF127-ICGD, HSA-LLP2A-ICGD, and HSA-ICGD. Figure 17 shows the mass spectra of the various HSA-conjugates analyzed by MALDI

mass spectrometry. The cell nuclei were stained with DAPI and examined under a confocal fluorescence microscope. Figure 18 shows the fluorescent images captured by the microscope, where the nuclei stained with DAPI appeared as blue spots, while the HSA-conjugates (ICGD) were distinctly visible as red fluorescence. The findings revealed minimal uptake of free ICGD and HSA-ICGD by the cells compared to the single ligand-conjugated constructs of HSA-LBF127-ICGD and HSA-LLP2A-ICGD. Most notably, the double ligand conjugated HSA-LBF127-LLP2A-ICGD exhibited most intense red fluorescence, suggesting the highest cellular uptake among all groups. Therefore, the fluorescent images indicate that the dual receptor targeting of HSA-LBF127-LLP2A-ICGD enables specific cellular uptake by EO771 cells for chemotherapeutic delivery.

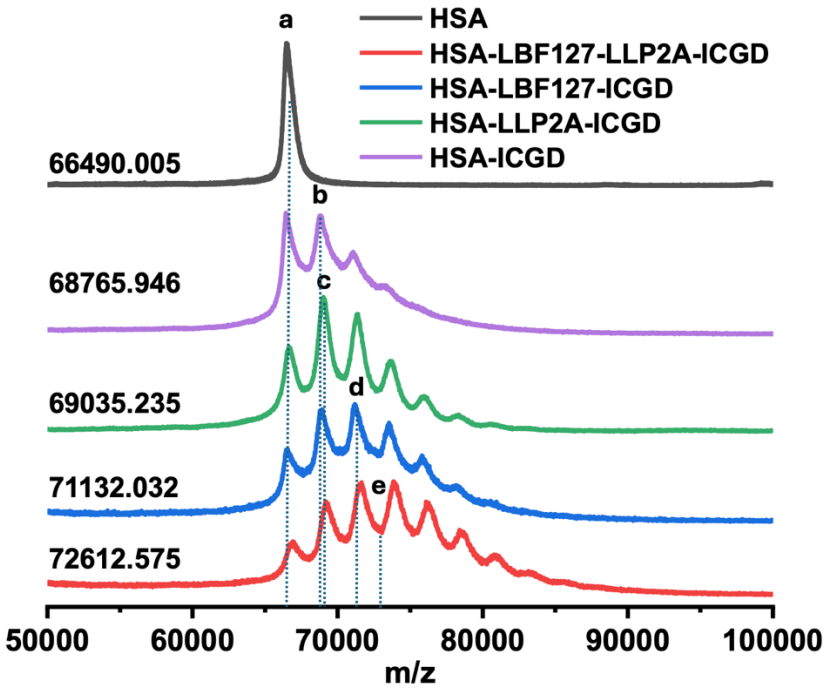

Figure 17: Mass Spectrometry confirming success of site-specific modification of HSA-conjugates used for in vitro and in vivo studies.

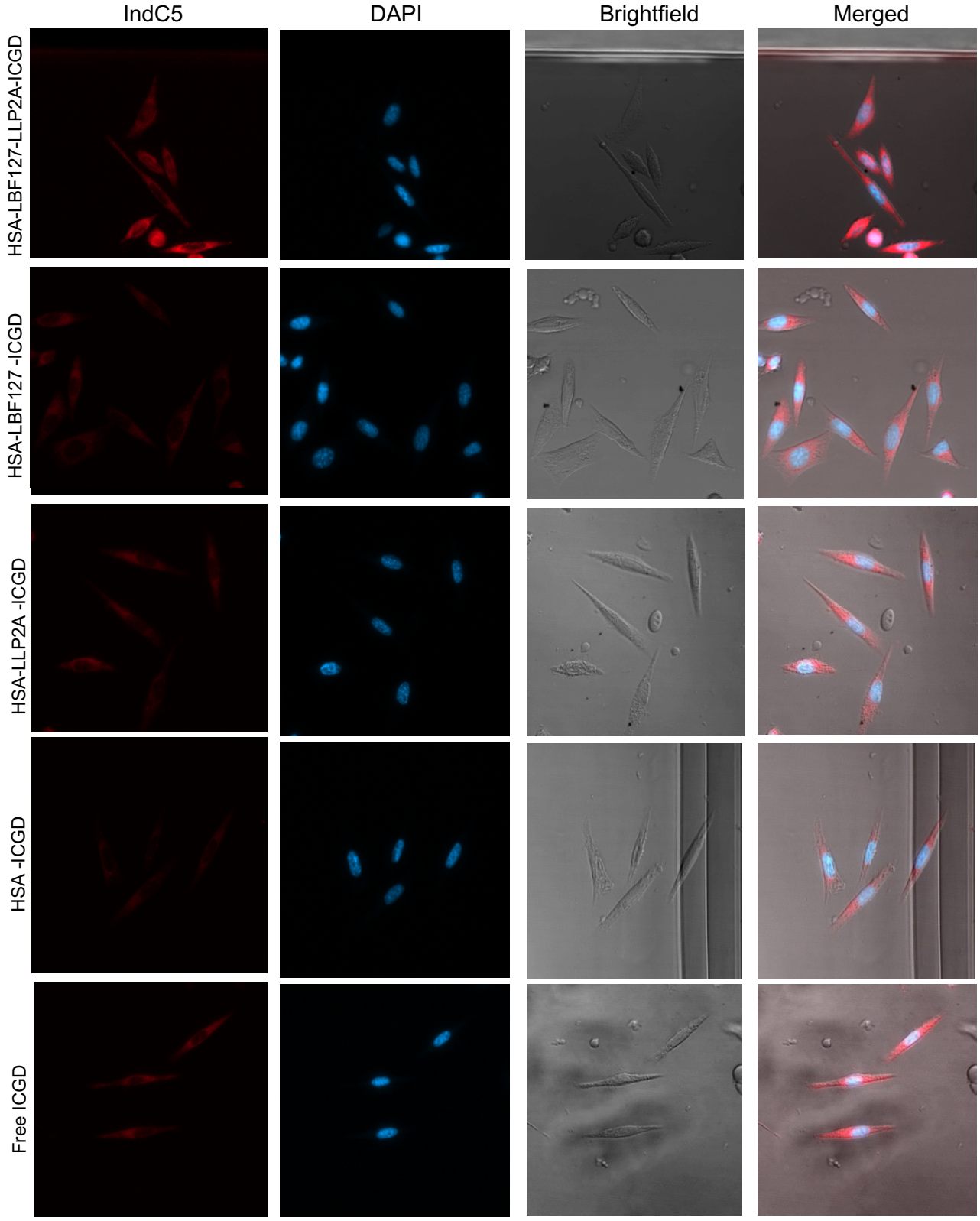

Figure 18: Fluorescence images of the cellular uptake of various HSA-nanoparticle formulations on EO771 cells (24 hr). IndC5 (red) wavelength parameter representative for HSA-ICGD conjugate tracking. DAPI staining (blue) indicates cell nucleus.

Kinetics of Cellular Uptake of HSA-conjugates by EO771 cells

In this study, we assessed the cellular uptake time course of dual targeting HSA-LBF127-LLP2A-ICGD conjugate by murine breast carcinoma (EO771) cells. Given the typically longer half-life of the HSA protein in circulation compared to our previously tested nanoparticles, we sought to investigate its distribution kinetics and binding affinity specific to this cell line's surface receptors. Cellular uptake activity was evaluated by measuring the fluorescence intensity of ICGD across the entire cross-section of individual live cells using confocal laser scanning microscopy over a period ranging between 0.5 to 24 hours. Representative images of ICGD positive cells are seen in EO771 (Fig. 19). Cellular uptake of LBF127-LLP2A-ICGD conjugate was apparent starting at the five-hour time point, and fluorescent signal continued to intensify over time. Cell nuclei of EO771 cells were labeled by DAPI (in blue).

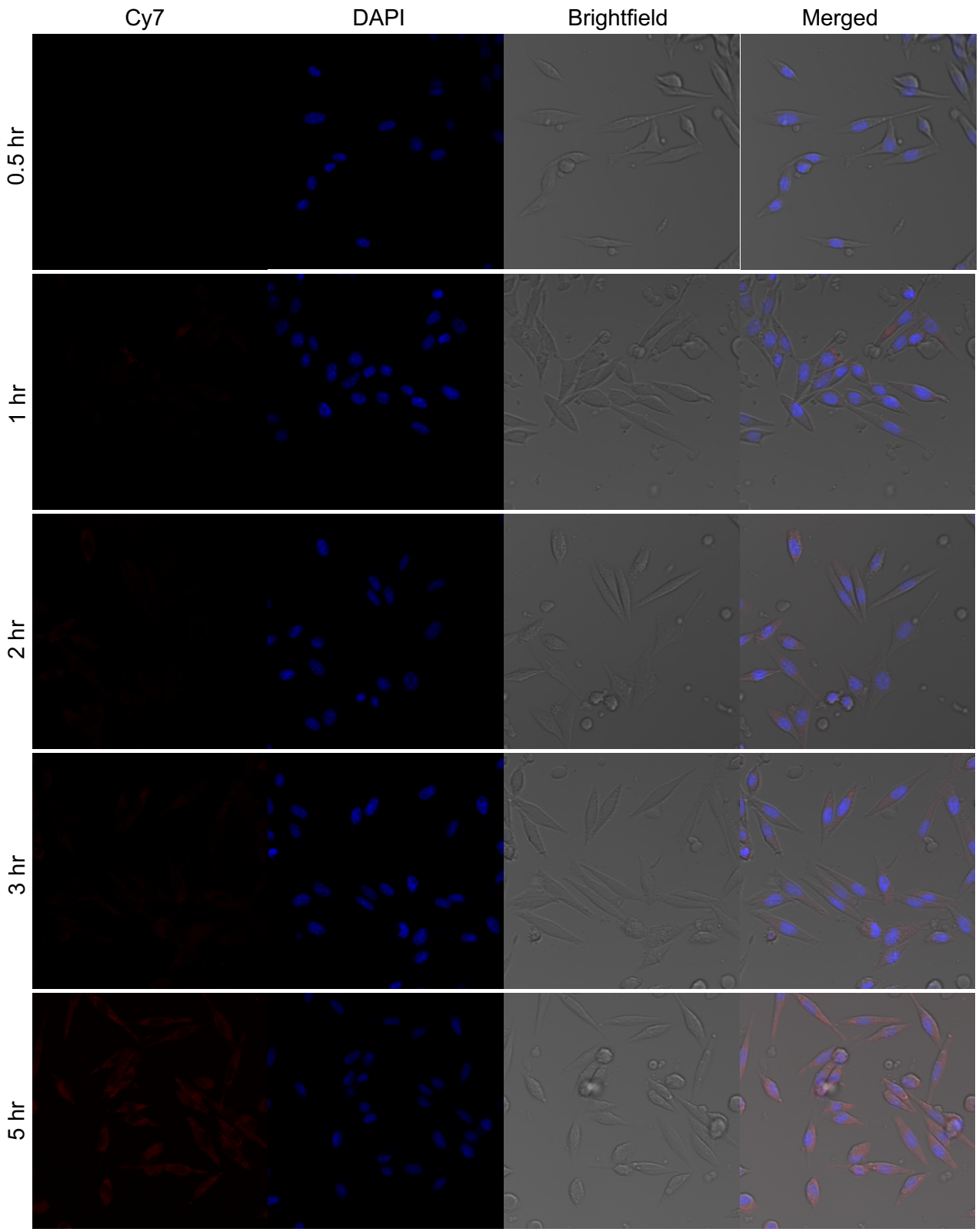
Cy7
DAPI
Brightfield
Merged
0.5 hr
1 hr
2 hr
3 hr
5 hr

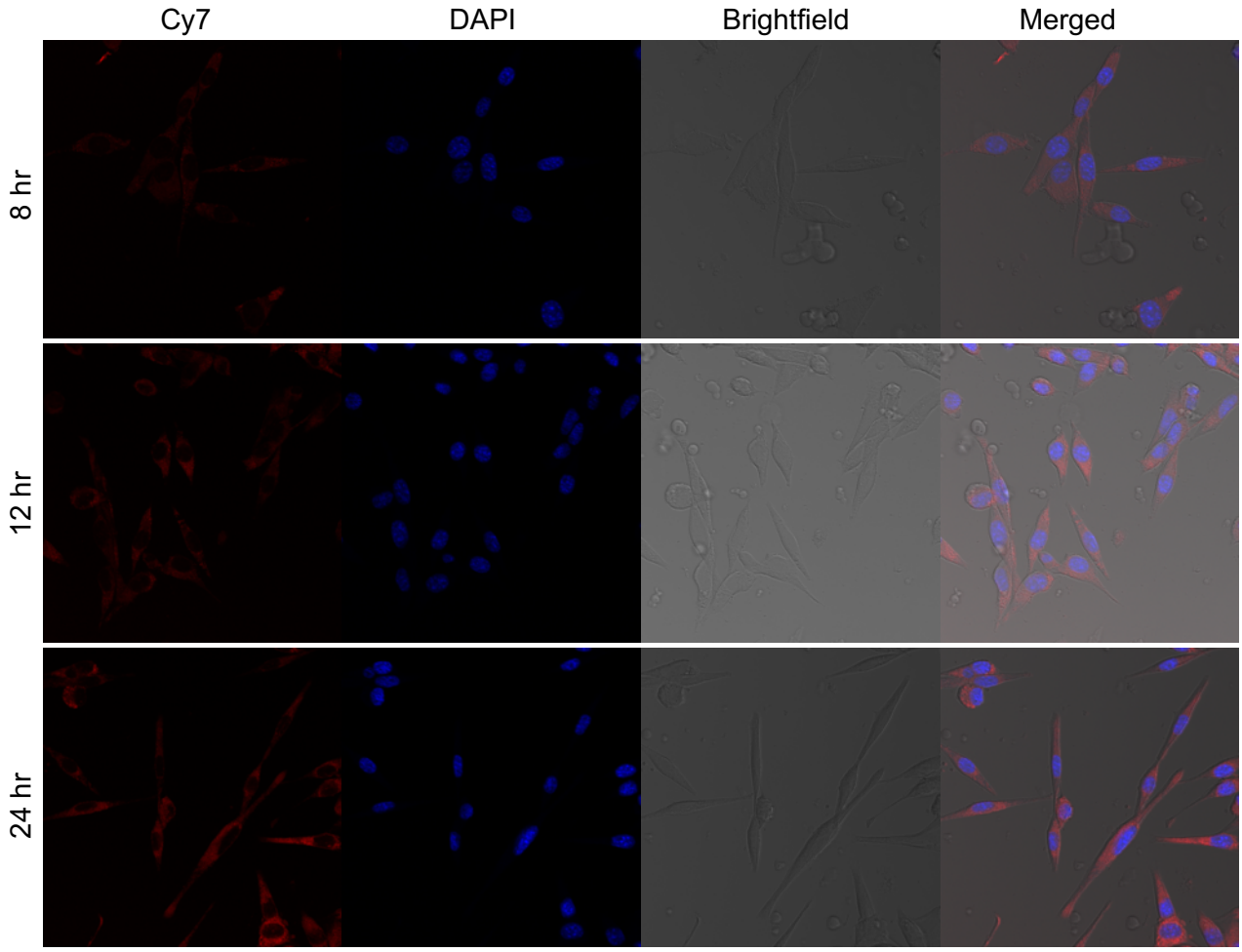

Figure 19: Time-dependent cellular uptake of HSA-LBF127-LLP2A-ICGD conjugate (in red) in EO771 exposed cells. Cell nuclei were labeled by DAPI in blue.

Half Maximal Effective Concentration Cytotoxicity Assay

The MTS assay was used to evaluate the cytotoxicity activity of the various BTZ-loaded HSA-conjugates and free BTZ on EO771 cells by measuring the conversion of formed formazan in the presence of phenazine methosulfate (PMS), which occurs in the mitochondria of metabolically active cells. Cell viability and proliferation was therefore quantified based on the intensity of the colored formazan product, which is directly proportional to the number of viable cells. We found that the EO771 cells only showed a significant and observable dose dependent change after 72 hours of incubation (Fig. 20), as compared to 24 and 48 hours incubation (data not shown) for the BTZ concentrations ranging between 5000-0.15 nM. Using the 72 hr drug exposure time, the half-maximal effective concentrations (EC_{50}) of HSA-LBF127-BTZ + HSA-LBF127-LLP2A, HSA-LBF127-BTZ, and free BTZ against EO771 cells in the MTS assay were determined to be 12.04 nM, 7.68 nM, and 3.24 nM respectively.

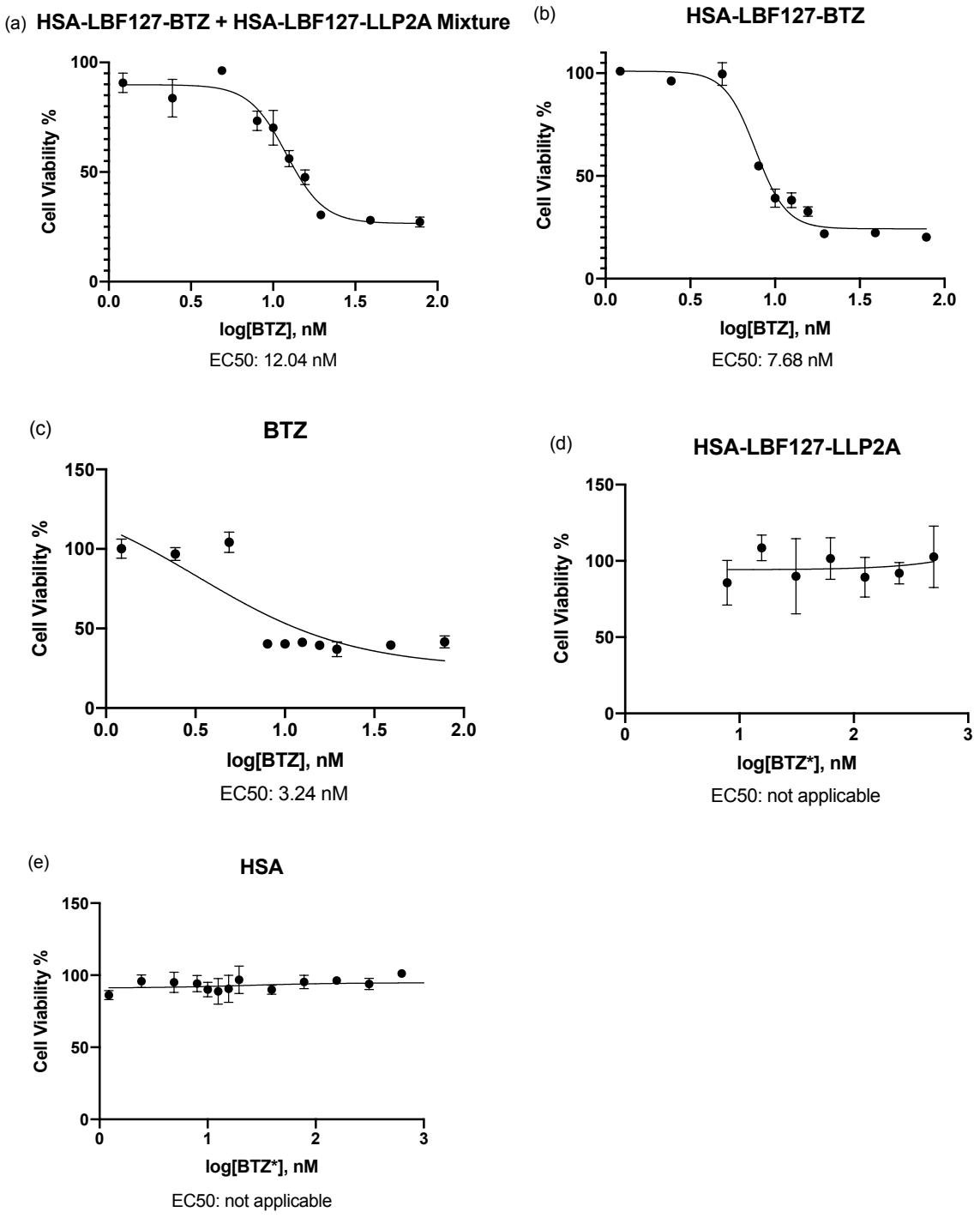

Figure 20: Percent Cell Viability from MTS/PMS Cytotoxicity Assay on EO771 Cells at 72 hours after exposure to different concentrations of various HSA-conjugates with or without covalent loading of BTZ. Panels a-c test a range of BTZ concentrations on EO771 cells. Panels d and e test the vehicle toxicity alone, without BTZ. However, concentrations of Log[BTZ*] was based on equivalent concentration of BTZ to HSA (4:1). EC50 values are calculated below each corresponding graph.

2.5. CONCLUSION

In this study, HSA-LBF127 conjugates were successfully discovered to target EO771 murine breast cancer cells. The effectiveness of HSA-LBF127 conjugates was evaluated by in vitro cellular uptake, cell specific binding, and kinetic cellular uptake for EO771 cells. The results revealed high cellular internalization of the HSA-LBF127 conjugates specific to murine breast cancer compared to other tested ligands and cell lines. These findings suggest that the chemically-defined targeting HSA-conjugates with drug-loading affinity element has great potential for targeted delivery of boronate-containing drugs (e.g., bortezomib) or prodrugs against breast cancer. Recent work by Luna et al.,[31] demonstrated that bortezomib can sensitize stem-like solid tumor cells for attack by natural killer cells. We believe the dual targeting HSA-LBF127-LLP2A-BTZ conjugate will be able to elicit significant anti-tumor NK cell response against EO771 breast cancer in a syngeneic model. There is significant potential in enhancing the immune system's defenses and effectively directing the chemotherapy drug bortezomib to attack breast cancer cells while sparing healthy breast epithelial cells. Further studies should be implemented on the toxicity of the HSA-LBF127-BTZ + HSA-LFB127-LLP2A mixture on natural killer cells, as well as biodistribution, therapeutic and mechanistic studies in vivo.

References

1. Sun L, Liu H, Ye Y, Lei Y, Islam R, Tan S, Tong R, Miao YB, Cai L. Smart nanoparticles for cancer therapy. Signal Transduct Target Ther. **2023** Nov 3;8(1):418. doi: 10.1038/s41392-023-01642-x. PMID: 37919282; PMCID: PMC10622502.
2. World Cancer Research Fund. "Bladder Cancer Statistics." World Cancer Research Fund, www.wcrf.org/cancer-trends/bladder-cancer-statistics/.
3. Saginala K, Barsouk A, Aluru JS, Rawla P, Padala SA, Barsouk A. Epidemiology of Bladder Cancer. Med Sci (Basel). **2020** Mar 13;8(1):15. doi: 10.3390/medsci8010015. PMID: 32183076; PMCID: PMC7151633.
4. Zhang H, Aina OH, Lam KS, de Vere White R, Evans C, Henderson P, Lara PN, Wang X, Bassuk JA, Pan CX. Identification of a bladder cancer-specific ligand using a combinatorial chemistry approach. Urol Oncol. **2012** Sep;30(5):635-45. doi: 10.1016/j.urolonc.2010.06.011. Epub 2010 Oct 2. PMID: 20888272; PMCID: PMC4572726.
5. Hong F, Park JS, Kim SW, Park SJ, Kim SK. Near-infrared phototherapy for patient-derived orthotopic xenograft model of hepatocellular carcinoma in combination with indocyanine green. J Photochem Photobiol B. **2020** Aug;209:111938. doi: 10.1016/j.jphotobiol.2020.111938. Epub 2020 Jun 14. PMID: 32590285.
6. Kubrak T, Karakuła M, Czop M, Kawczyk-Krupka A, Aebisher D. Advances in Management of Bladder Cancer-The Role of Photodynamic Therapy.

Molecules. **2022** Jan 23;27(3):731. doi: 10.3390/molecules27030731. PMID: 35163996; PMCID: PMC8838614.

7. Garcia-Mouronte E, Berna-Rico E, de Nicolas-Ruanes B, Azcarraga-Llobet C, Alonso-Martinez de Salinas L, Bea-Ardebol S. Imiquimod as Local Immunotherapy in the Management of Premalignant Cutaneous Conditions and Skin Cancer. Int J Mol Sci. **2023** Jun 29;24(13):10835. doi: 10.3390/ijms241310835. PMID: 37446011; PMCID: PMC10341632.
8. Okobi TJ, Uhomoibhi TO, Akahara DE, Odoma VA, Sanusi IA, Okobi OE, Umana I, Okobi E, Okonkwo CC, Harry NM. Immune Checkpoint Inhibitors as a Treatment Option for Bladder Cancer: Current Evidence. Cureus. **2023** Jun 6;15(6):e40031. doi: 10.7759/cureus.40031. PMID: 37425564; PMCID: PMC10323982.
9. Margarete Schön, Anne B. Bong, Claudia Drewniok, Jeannine Herz, Christoph C. Geilen, Julia Reifenberger, Bernd Benninghoff, Herbert B. Slade, Harald Gollnick, Michael P. Schön, Tumor-Selective Induction of Apoptosis and the Small-Molecule Immune Response Modifier Imiquimod, *JNCI: Journal of the National Cancer Institute*, Volume 95, Issue 15, 6 August **2003**, Pages 1138–1149.
10. Hsu MA, Okamura SM, De Magalhaes Filho CD, Bergeron DM, Rodriguez A, West M, Yadav D, Heim R, Fong JJ, Garcia-Guzman M. Cancer-targeted photoimmunotherapy induces antitumor immunity and can be augmented by anti-PD-1 therapy for durable anticancer responses in an immunologically active murine tumor model. Cancer Immunol Immunother. **2023** Jan;72(1):151-

168. doi: 10.1007/s00262-022-03239-9. Epub 2022 Jul 1. PMID: 35776159; PMCID: PMC9813181.

11. Jackson Laboratory. "Physiological Data." Jackson Laboratory, https://jackson.jax.org/rs/444-BUH-304/images/physiological_data_001800.pdf.

12. Taconic Biosciences. "FVB Mouse Strain." Taconic Biosciences, www.taconic.com/products/mouse-rat/standard-strains-and-stocks/fvb#tabsmobiledropdown-4917198966-item-15b633d1d7-tab.

13. Schneck K, Washington M, Holder D, Lodge K, Motzel S. Hematologic and serum biochemical reference values in nontransgenic FVB mice. Comp Med. **2000** Feb;50(1):32-5. PMID: 10987664.

14. Wagstaff, A.J., Perry, C.M. Topical Imiquimod. *Drugs* 67, 2187–2210 (**2007**). https://doi.org/10.2165/00003495-200767150-00006

15. Gill E, Perks CM. Mini-Review: Current Bladder Cancer Treatment-The Need for Improvement. Int J Mol Sci. **2024** Jan 26;25(3):1557. doi: 10.3390/ijms25031557. PMID: 38338835; PMCID: PMC10855537.

16. Kaufman DS. Challenges in the treatment of bladder cancer. Ann Oncol. **2006** May;17 Suppl 5:v106-12. doi: 10.1093/annonc/mdj963. PMID: 16807436.

17. Davide Bedognetti, Ena Wang, Marimo Sato-Matsushita, Francesco M. Marincola, Maria Libera Ascierto, Chapter 23 - Molecular Profiling of Immunotherapeutic Resistance, Editor(s): George C. Prendergast, Elizabeth M. Jaffee, Cancer Immunotherapy (Second Edition), Academic Press, **2013**,

Pages 373-394, ISBN 9780123942968, https://doi.org/10.1016/B978-0-12-394296-8.00023-3.

18. GBD 2019 Cancer Risk Factors Collaborators. The global burden of cancer attributable to risk factors, 2010-19: a systematic analysis for the Global Burden of Disease Study 2019. Lancet. **2022** Aug 20;400(10352):563-591. doi: 10.1016/S0140-6736(22)01438-6. PMID: 35988567; PMCID: PMC9395583.

19. Alkabban FM, Ferguson T. Breast Cancer. [Updated 2022 Sep 26]. In: StatPearls [Internet]. Treasure Island (FL): StatPearls Publishing; **2024** Jan-. Available from: https://www.ncbi.nlm.nih.gov/books/NBK482286/

20. Bansal, S.; Vu, K.; Liu, R.; Ajena, Y.; Xiao, W.; Menon, S. M.; Bennett, A.; Gelli, A.; Lam, K. S. Discovery and Characterization of a Potent Antifungal Peptide through One-Bead, One-Compound Combinatorial Library Screening. *ACS Infect. Dis.* **2022**, *8*, 1291– 1302, DOI: 10.1021/acsinfecdis.2c00019

21. Hao D, Ma B, He C, Liu R, Farmer DL, Lam KS, Wang A. Surface modification of polymeric electrospun scaffolds via a potent and high-affinity integrin α4β1 ligand improved the adhesion, spreading and survival of human chorionic villus-derived mesenchymal stem cells: a new insight for fetal tissue engineering. J Mater Chem B. **2020** Feb 26;8(8):1649-1659. doi: 10.1039/c9tb02309g. PMID: 32011618; PMCID: PMC7353926.

22. Alwahsh M, Farhat J, Talhouni S, Hamadneh L, Hergenröder R. Bortezomib advanced mechanisms of action in multiple myeloma, solid and liquid tumors

along with its novel therapeutic applications. EXCLI J. **2023** Jan 16;22:146-168. doi: 10.17179/excli2022-5653. PMID: 36998701; PMCID: PMC10043448.

23. Irvin WJ Jr, Orlowski RZ, Chiu WK, Carey LA, Collichio FA, Bernard PS, Stijleman IJ, Perou C, Ivanova A, Dees EC. Phase II study of bortezomib and pegylated liposomal doxorubicin in the treatment of metastatic breast cancer. Clin Breast Cancer. **2010** Dec 1;10(6):465-70. doi: 10.3816/CBC.2010.n.061. PMID: 21147690; PMCID: PMC5830095.

24. Paolini R, Molfetta R. Dysregulation of DNAM-1-Mediated NK Cell Anti-Cancer Responses in the Tumor Microenvironment. Cancers (Basel). **2023** Sep 18;15(18):4616. doi: 10.3390/cancers15184616. PMID: 37760586; PMCID: PMC10527063.

25. Fingar VH. Vascular effects of photodynamic therapy. J Clin Laser Med Surg. **1996** Oct;14(5):323-8. doi: 10.1089/clm.1996.14.323. PMID: 9612199.

26. Raut CP, Sethi KS, Kohale BR, Mamajiwala A, Warang A. Indocyanine green-mediated photothermal therapy in treatment of chronic periodontitis: A clinico-microbiological study. J Indian Soc Periodontol. **2018** May-Jun;22(3):221-227. doi: 10.4103/jisp.jisp_128_18. PMID: 29962701; PMCID: PMC6009169.

27. Friedrich V, Choi HW. The Urinary Microbiome: Role in Bladder Cancer and Treatment. Diagnostics (Basel). **2022** Aug 26;12(9):2068. doi: 10.3390/diagnostics12092068. PMID: 36140470; PMCID: PMC9497549.

28. Xiao W, Ma W, Wei S, Li Q, Liu R, Carney RP, Yang K, Lee J, Nyugen A, Yoneda KY, Lam KS, Li T. High-affinity peptide ligand LXY30 for targeting α3β1 integrin in non-small cell lung cancer. J Hematol Oncol. 2019 Jun

10;12(1):56. doi: 10.1186/s13045-019-0740-7. Erratum in: J Hematol Oncol. **2019** Jul 26;12(1):83. PMID: 31182116; PMCID: PMC6558829.

29. Zhou B, Gibson-Corley KN, Herndon ME, Sun Y, Gustafson-Wagner E, Teoh-Fitzgerald M, Domann FE, Henry MD, Stipp CS. Integrin α3β1 can function to promote spontaneous metastasis and lung colonization of invasive breast carcinoma. Mol Cancer Res. **2014** Jan;12(1):143-154. doi: 10.1158/1541-7786.MCR-13-0184. Epub 2013 Sep 3. PMID: 24002891; PMCID: PMC3947021.
30. Yu X, Ruan M, Wang Y, Nguyen A, Xiao W, Ajena Y, Solano LN, Liu R, Lam KS. Site-Specific Albumin-Selective Ligation to Human Serum Albumin under Physiological Conditions. Bioconjug Chem. **2022** Dec 21;33(12):2332-2340. doi: 10.1021/acs.bioconjchem.2c00361. Epub 2022 Nov 9. PMID: 36350013; PMCID: PMC9782315.
31. Luna JI, Grossenbacher SK, Sturgill IR, Ames E, Judge SJ, Bouzid LA, Darrow MA, Murphy WJ, Canter RJ. Bortezomib Augments Natural Killer Cell Targeting of Stem-Like Tumor Cells. Cancers (Basel). **2019** Jan 14;11(1):85. doi: 10.3390/cancers11010085. PMID: 30646520; PMCID: PMC6356940.